# 单相、两相传热强化技术及其进展
# (Focus on tube side)

**Chi-Chuan Wang (王啟川), PhD, FASME, FASHRAE**

**Professor, Department of Mechanical Engineering,**

**National Chiao Tung University, Hsinchu, Taiwan**

**E-mail: ccwang@mail.nctu.edu.tw**

**Dec. 1, 2017 @ 珠海格力电器**

# Outline

- 基本背景
- 定性選擇方法
- 一些觀念之澄清
- 定量性能評估
- 熱傳增強與熱傳管之選用
  - 基本概念
  - Boundary Layer Restarting
    - Intrusion design
    - Grooved design
  - Swirled Flow
  - Highly enhanced surface used for phase change
- Conclusions

# 典型氣冷式熱交換器的熱流現象

- 熱傳分析
  - 管側冷媒熱傳
    - 平滑管
    - 微鰭管
    - 增強管
      - 兩相冷凝熱傳
      - 兩相蒸發熱傳
      - 單相熱傳
      - 兩相流譜
      - 壓降
      - 新冷媒熱傳

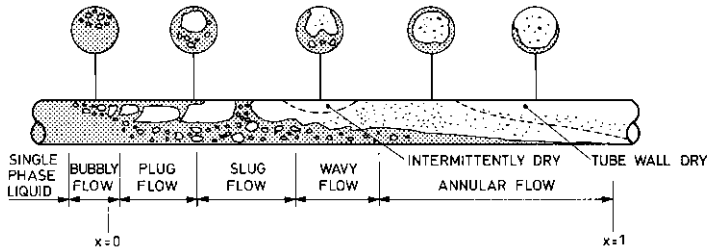


管內兩相流譜之變化

  - 鰭片側空氣熱傳
    - 乾盤管 (室外機)
    - 濕盤管 (室內機)
      - 平板鰭片
      - 百葉窗鰭片
      - 波浪鰭片
      - Convex-Louver鰭片
      - Lanced 鰭片
      - 親水性鰭片

# 熱交換原理

總阻抗：$R=R_A+R_W+R_B$

熱通量q

$q=(T_A-T_B)/R$

$Q=q \cdot A \Rightarrow$ 總熱傳量

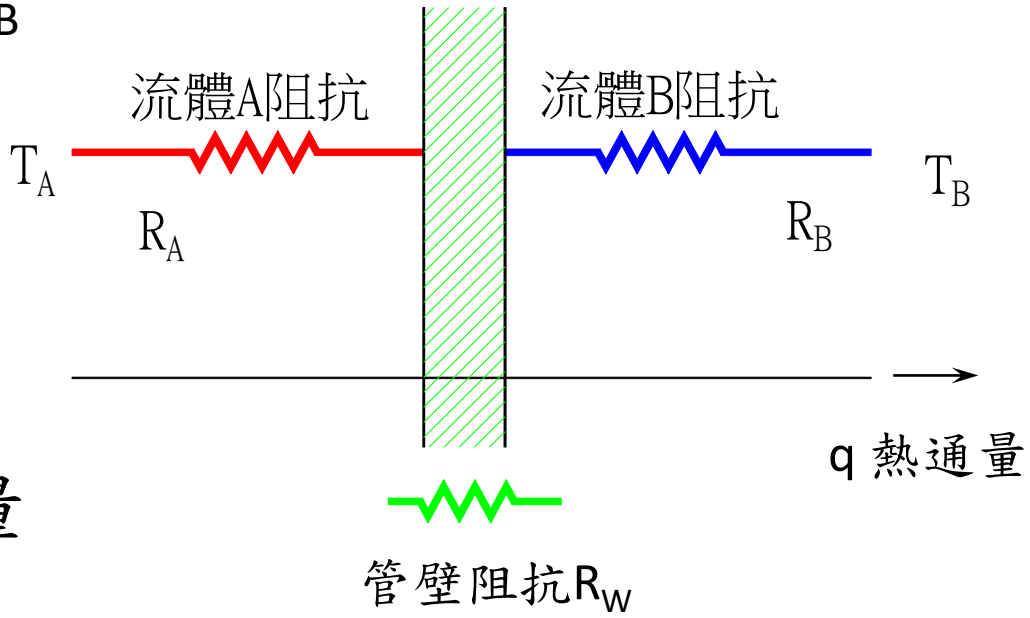


因此若能確切掌握流體阻抗，
即能精確設計熱交換器。

# Fundamentals of Heat Transfer

$$Q = UA\Delta T, \quad \frac{1}{UA} = \frac{1}{\eta_o h_o A_o} + \frac{\delta_w}{k_w A_w} + \frac{1}{h_i A_i}$$

$$or \quad Q = \eta_o h_o A_o \Delta T \text{ for electronic cooling}$$

- U: overall heat transfer coefficient
  - $h_i$, $h_o$: inside & outside heat transfer coefficient
  - $\eta_o$: surface efficiency ($=1-A_f/A_o(1-\eta_f)$)
  - $\eta_f$: fin efficiency
- A: surface area
- $\Delta T$: effective Temperature Difference

  For Heat Transfer Augmentation. One needs to..

  (a) Increase A? (Most effective but limited by $\Delta P$)

  (b) Increase U? (Effective but also prone to increasing $\Delta P$)

  (c) What else can one do? (Manipulating $\Delta T$?)

# 總熱傳係數

所以若原熱交換器無鰭片的話，熱傳的阻抗方程式如下：

$$\frac{1}{UA} = \frac{1}{h_1 A_{w1}} + \frac{\Delta X}{kA} + \frac{1}{h_2 A_{w2}}$$

總阻抗　熱側阻抗　管壁阻抗　冷側阻抗

若有鰭片時，則阻抗方程式改寫如下：

$$\frac{1}{UA} = \underbrace{\frac{1}{\eta_1 h_1 A_{w1}}}_{\text{熱側阻抗}} + \frac{\Delta X}{kA} + \underbrace{\frac{1}{\eta_2 h_2 A_{w2}}}_{\text{冷側阻抗}}$$

總阻抗　管壁阻抗

# 例：鰭管式熱交換器阻抗分布

- 以空調常用的氣冷式冷凝器的相關應用而言，$h_i \approx 2000\ \mathrm{W/m^2 \cdot K}$，$h_o \approx 50\ \mathrm{W/m^2 \cdot K}$，$\eta_s \approx 0.7$ (請注意上述值只是在一種操作條件下的近似值，不可隨意將此值拿來運用於各種不同的應用場合上)。

假設 $A_i$ 為一單位面積 ( = 1 $\mathrm{m^2}$)，而設 $A_o/A_i$ =10，故 $A_o$ =10 $\mathrm{m^2}$ ，總熱傳係數 $U$ 的參考面積為$A_o$，則

$$\therefore \frac{1}{U_o A_o} = \frac{1}{2000\, A_i} + \frac{1}{0.7 \times 50\, A_o} = \frac{1}{2000\, A_i} + \frac{1}{35 A_o} = \frac{0.0005}{A_i} + \frac{0.0286}{A_o}$$

$$\Rightarrow \frac{1}{U_o} = 0.005(\text{管內阻抗}) + 0.0286(\text{管外阻抗}) = 0.0336 K \cdot m^2 / W$$

$$\Rightarrow U_o = 29.77\ \mathrm{W/m^2 \cdot K}$$

⇒管內的阻抗約佔 15% (0.005/0.0336)，

⇒而管外阻抗約佔85%。氣冷式熱交換器的熱傳阻抗幾乎都是落在空氣側

- 殼管式熱交換器的殼側與管側流體之熱傳係數均為幾千大小，其熱傳阻抗約佔有同等重要地位。

# 例：鰭管式熱交換器阻抗分布 (Conti.)

◆Case 1： 上述例題如將空氣側熱傳係數提高一倍，即 $h_i \approx 2000$ W/m$^2$·K，$h_o \approx 100$ W/m$^2$·K，$\eta_s \approx 0.65$ (請注意空氣側熱傳係數增加，則鰭片效率會跟著降低，為什麼(想一想原因)?)。

假設 $A_i$ 為一單位面積 ( = 1 m$^2$)，而設 $A_o/A_i$ =10，故 $A_o$ =10 m$^2$ ，總熱傳係數 $U$ 的參考面積為$A_o$，則

$$\therefore R_t = \frac{1}{U_o A_o} = \underbrace{\frac{1}{2000 A_i}}_{\text{冷媒側阻抗}} + \underbrace{\frac{1}{0.65 \times 100 A_o}}_{\text{空氣側阻抗}} = \frac{1}{2000 A_i} + \frac{1}{65 A_o} = \frac{0.0005}{A_i} + \frac{0.0154}{A_o}$$

總阻抗

$$\Rightarrow R_t = \frac{1}{U_o A_o} = 0.0005(\text{管內阻抗}) + 0.00154(\text{空氣側阻抗}) = 0.00204 K \cdot m^2 / W$$

$$\Rightarrow \frac{1}{U_o} = 0.0204 K \cdot m^2 / W \quad \Rightarrow U_o = 49.02 W / m^2 \cdot K$$

➔管內的阻抗約佔25% (0.0005/0.00204)，

➔而空氣側阻抗約佔75%。

◆總熱傳係數比值 49.02/29.77=1.65，意味著如果兩側流體的溫差不變，則空氣側熱傳係數增加一倍，可提升熱傳量約65%。

# 例:鰭管式熱交換器阻抗分布 (Conti.)

◆ Case 2：上述例題如將冷媒側熱傳係數提高一倍，即 $h_i \approx 4000$ W/m$^2$·K，$h_o \approx 50$ W/m$^2$·K，$\eta_s \approx 0.70$ (請注意冷媒側熱傳係數增加，原來的鰭片效率並不會跟著改變，為什麼(想一想原因)?)。

假設 $A_i$ 為一單位面積 ( = 1 m$^2$)，而設 $A_o/A_i$ =10，故 $A_o$ =10 m$^2$ ，總熱傳係數 $U$ 的參考面積為$A_o$，則

$$\therefore R_t = \frac{1}{U_o A_o} = \underbrace{\frac{1}{4000 A_i}}_{\text{冷媒側阻抗}} + \underbrace{\frac{1}{0.70 \times 50 A_o}}_{\text{空氣側阻抗}} = \frac{1}{4000 A_i} + \frac{1}{35 A_o} = \frac{0.00025}{A_i} + \frac{0.0286}{A_o}$$

總阻抗

$$\Rightarrow R_t = \frac{1}{U_o A_o} = 0.00025(\text{管內阻抗}) + 0.00286(\text{空氣側阻抗}) = 0.00311 K \cdot m^2 / W$$

$$\Rightarrow \frac{1}{U_o} = 0.0311 K \cdot m^2 / W \quad \Rightarrow U_o = 32.15 W / m^2 \cdot K$$

➔管內的阻抗約佔8.0% (0.00025/0.00311)，

➔而空氣側阻抗約佔92%。

◆總熱傳係數比值 32.15/29.77=1.08，意味著如果兩側流體的溫差不變，則冷媒側熱傳係數增加一倍，可提升熱傳量約8%。

# Stop & Think

- Question
  - 兩熱交換器，型式完全一樣，幾何尺寸相同，一使用銅，一使用鈦，如果工作流體相同，流量相同，則
    - 兩熱交換器的熱傳量，何者較大？
    - 兩熱交換器的熱傳性能(以熱傳係數而言)，何者較佳？
    - 兩熱交換器的壓損，何者較大？

# 熱交換器選擇考量因素

- 熱流需求：包括熱交換量、工作流體的溫度、壓力與可允許的壓損，選擇的熱交換器當然必須滿足這些熱流的基本需求；且熱交換器能在工作溫度壓力下長期運作，能忍受因溫差所產生的熱應力影響，應力主要由入口壓力與溫度差所引起，常見各種熱交換器所能忍受的最大壓力與溫度範圍大致如下
- 熱交換器與流體的匹配性：熱交換器的材料必須與工作流體能長期搭配，無腐蝕的問題；其中必須特別注意結垢的影響，設計上應同時考慮正常操作設計點下與非設計點上運作時，結垢在不同溫度壓力變化下的影響，一般而言，典型氣對氣熱交換器的結垢影響較小，這是因為許多製程的應用上，氣體多半比液體來的乾淨，而且如果使用轉輪式的再生式熱交換器，氣體在不同時間時相反方向的流動也有助於熱交換器本身的自清，因此結垢的影響相對比液體側小；不過此類再生式熱交換器也因氣體交互流過熱交換器而可能產生污染問題。

# 熱交換器選擇考量因素 (Conti.)

- 流體型式：由於氣體體的熱傳係數遠低於液體，因此氣對氣熱交換器通常需非常大的熱交換面積，一般的作法乃藉由增加鰭片、縮小水力直徑與使用小管徑熱傳管來增加面積的密集度，密集度增加同時增加流動壓損，氣側壓損的影響相對於液體測重要很多，設計上必須特別注意。對液對液的熱交換而言，為了避免交叉感染的影響，通常不應該考慮使用再生式熱交換器，相較於氣對氣熱交換器，液對液熱交換器的壓損影響較小。對氣對液的熱交換器而言，由於氣側的熱傳係數遠低液體側，因此設計上的初步原則為盡量平衡兩側的熱傳性能(即 $\eta_o h_o A_o \sim \eta_i h_i A_i$)。
- 維護性：設計時必須考量停機清理與置換的問題；同時應留意製程應用條件改變時所帶來的影響。
- 造價：造價為選擇設非常重要的因素，例如板式熱交換器的造價會比殼管式熱交換器大，但是如果同時考量裝置、操作、維護等成本的影響，板式熱交換器成本可能反而比較便宜。設計上如果比較在意長期操作的成本，則在設計上就必須特別留意流動的壓損而非純粹的熱傳考慮。
- 空間與重量：許多應用上必須考慮到裝置時空間與重量的問題，例如熱交換器裝置於高樓層的重量負荷或是都會區維護空間缺乏的現實問題。

# 熱交換器的選擇原則（初步定性）

- Maximum Pressure
- Temperature range
- Fluids limitation
- Size range available
- Fouling & cleanability
- Plot area available
- Design life
- Location (maintenance)
- Is there a “temperature cross?”. If so, HX approaches counter flow is more appropriate

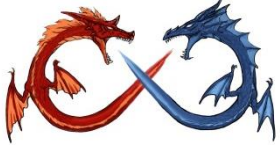

# 一些值得商榷的觀念

# ε-NTU 關係是否已飽和？

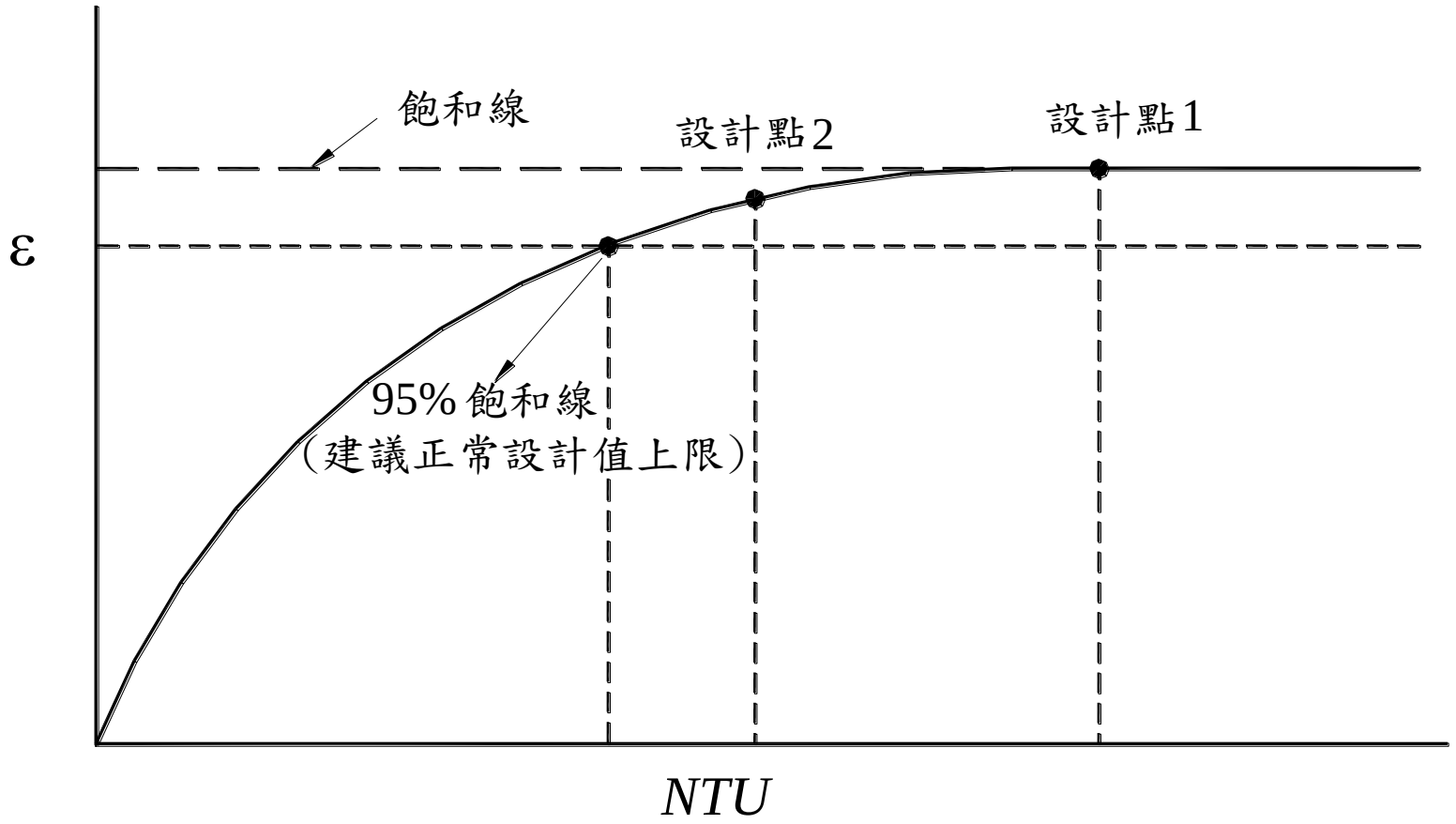

# 熱交換器越大熱傳效果越好？

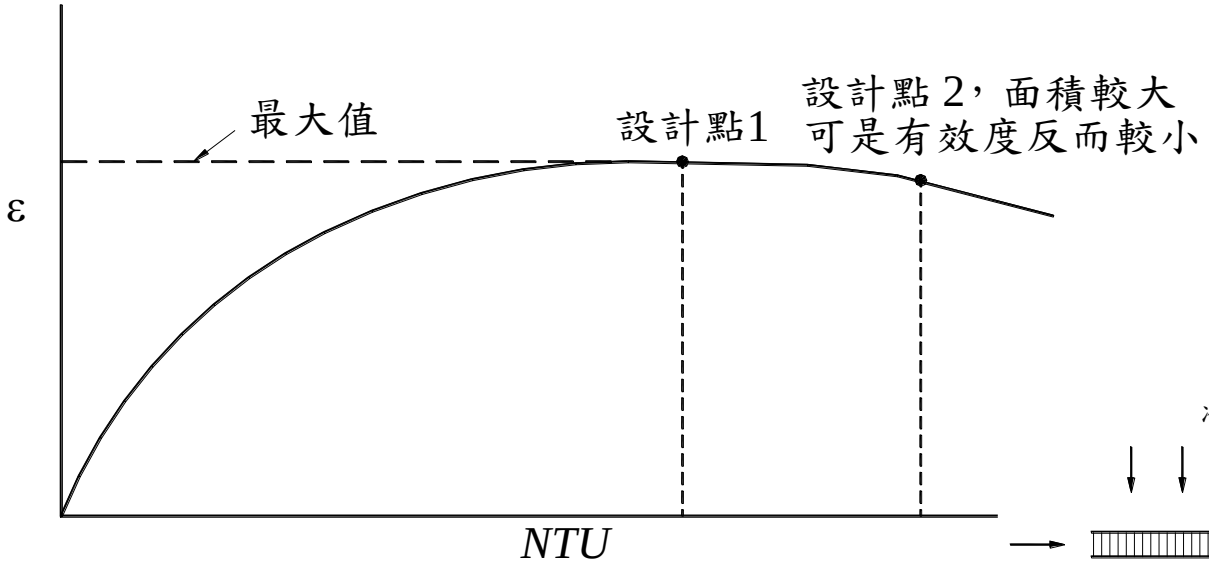


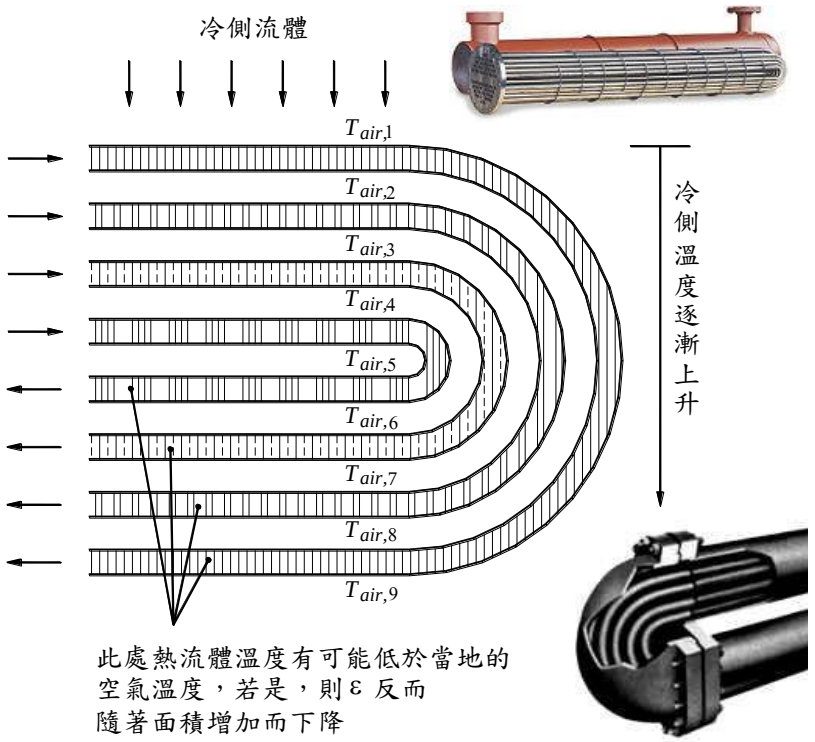

TABLE 11.7

| | |
|---|---|
| Crossflow<br>2 Passes<br>Infinite channels/tube rows in both streams<br>$(\dot{M}c_p)_{smaller}$ in either stream<br>–<br>Unmixed/unmixed<br>Mixed/mixed | CRO-UNMIX-MP-CO-1 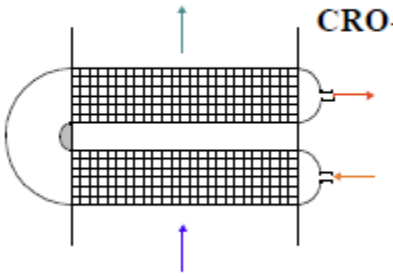 |

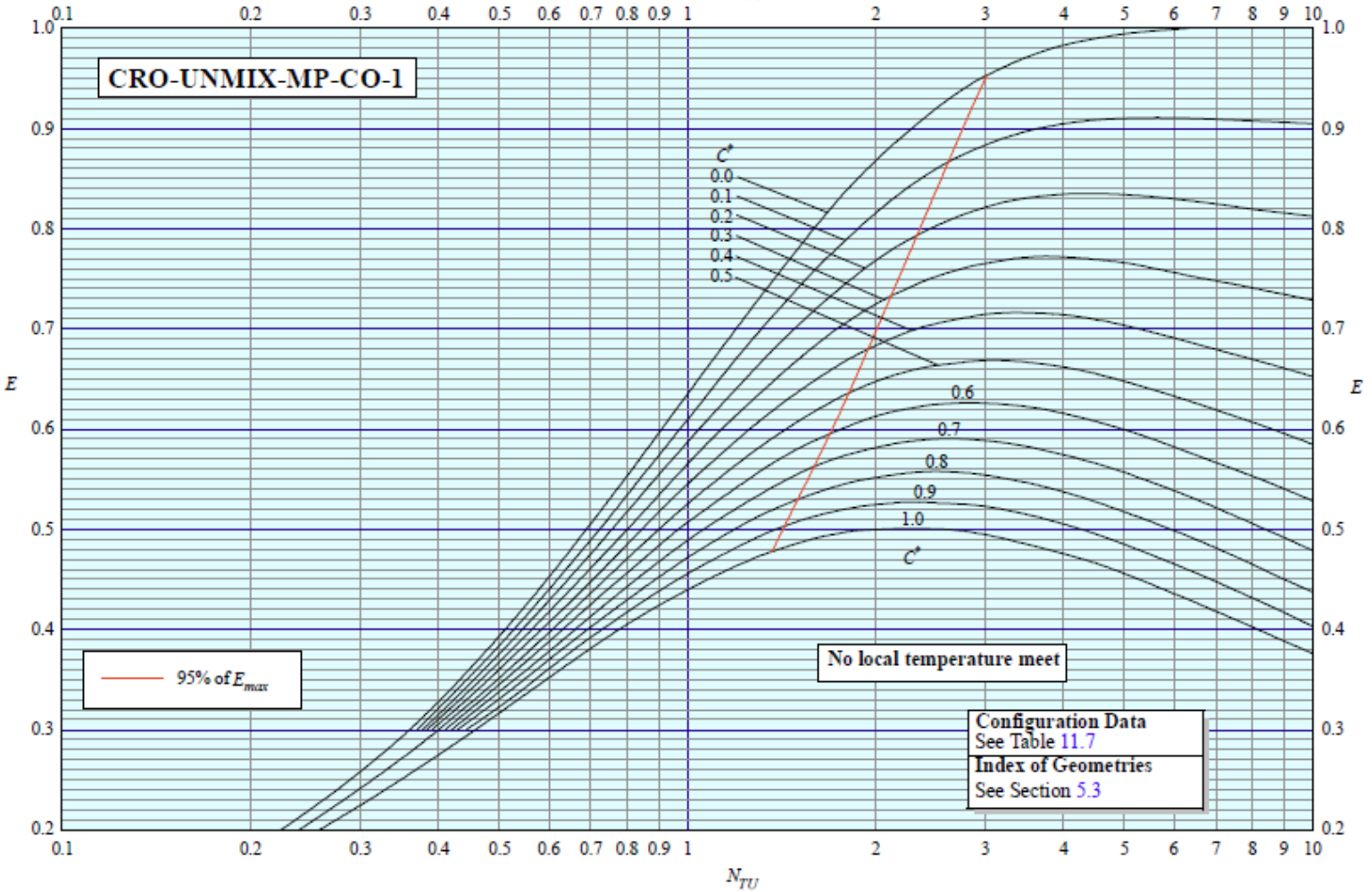


FIGURE 9 TWO-PASS CROSSFLOW WITH CO-CURRENT FLOW, BOTH STREAMS MIXED BETWEEN PASSES

# A Quick Overview of Compact Air-Cooled Heat Sinks Applicable for Electronic Cooling—Recent Progress, Inventions 2017, 2, 5; doi:10.3390/inventions2010005

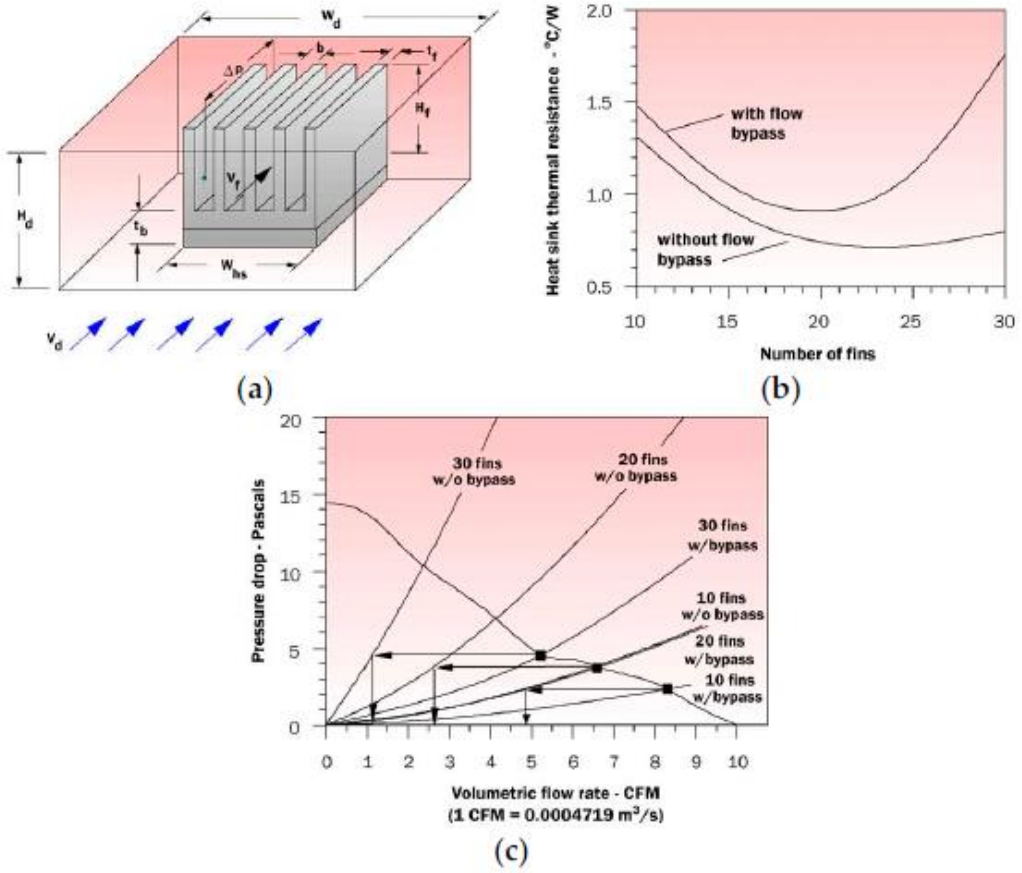


Figure 2. Effect of bypass and fin number on the thermal performance of a heat sink [16] with permission from Electronics Cooling / ITEM Media. (a) Schematic of airflow into a parallel plate fin heat sink with flow bypass; (b) Effect of number of fins on heat sink thermal resistance with and without flow bypass; (c) Heat sink pressure drop curves (with and without flow bypass) and fan curve with flow operating points. CFM is flow rate in English unit (cubic feet per minute).

# 熱交換器設計是否僅考慮熱傳量？

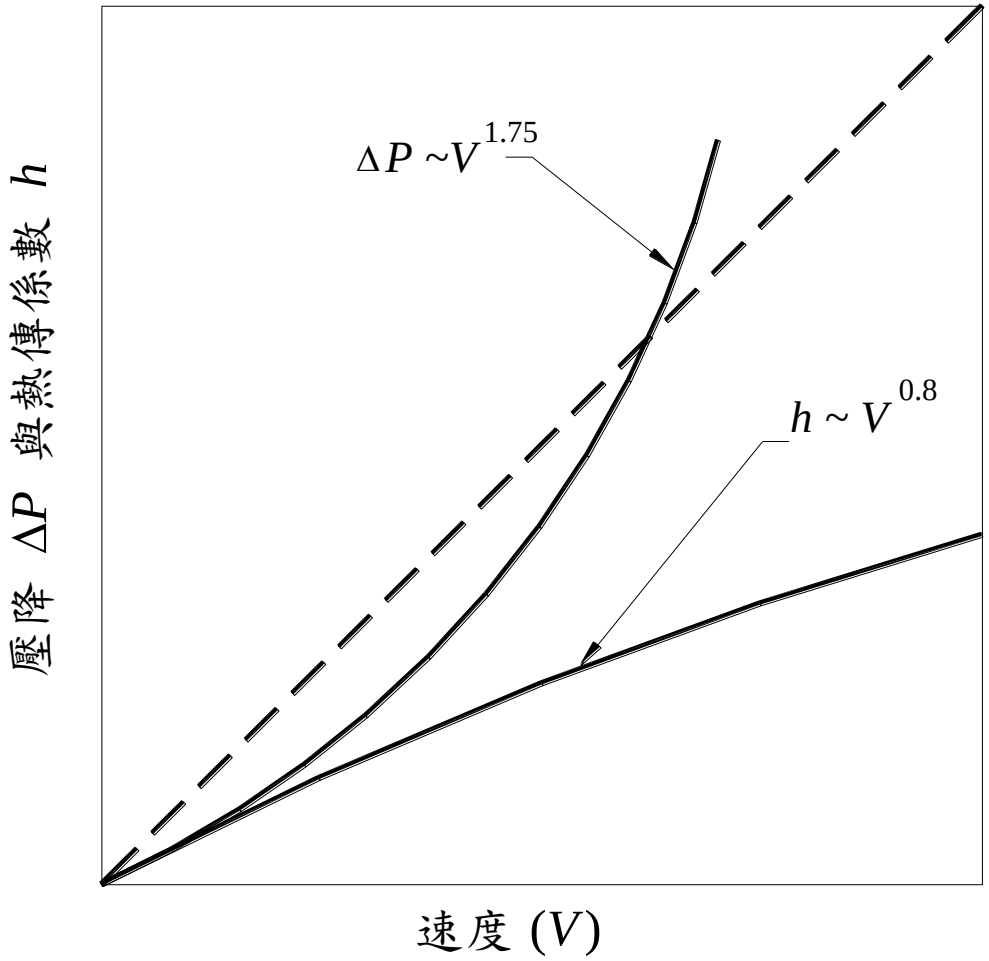


熱傳係數、壓降與速度的關係示意圖

# 熱傳增強管與熱傳增強鰭片使用的迷思

熱交換器性能評價方法 (Performance evaluation criteria)，使用熱傳增強管與熱傳增強鰭片來取代原有熱交換器的目的有四：

- 在維持相同的熱傳量且不增加壓降的條件下，如何減少熱交換器的面積。
- 在維持相同的熱傳量與原有熱交換器的面積下，如何降低流體間的有效溫差(或*LMTD*)。
- 在維持原有熱交換器的面積下，如何增加熱傳量。
- 在維持相同的熱傳量與原有熱交換器的面積下，如何減少流體通過熱交換器的壓降(即減少pumping power)。

- *FG*法則 (fixed geometry criteria)：適用於截面積與管長固定條件。*FG*法則可用於1對1直接置換式的應用，因為新的熱交換器與舊有的熱交換器一樣大。
- *FN*法則 (fixed number of tubes geometry criteria)：適用於截面積固定，但管長可允許變化。
- *VG*法則 (variable geometry criteria)：適用於熱傳量固定，但要適度的減少熱交換器的面積。

## PEC的應用法則與目的

| 法則 | 幾何參數 | 固定參數 | | | | 目的 |
|---|---|---|---|---|---|---|
| | | $\dot{m}$ | $W$ | $Q$ | $\Delta T$ | |
| FG-1a | $N$，$L$ | ☆ | | | ☆ | $\uparrow Q$ |
| FG-1b | $N$，$L$ | ☆ | | ☆ | | $\downarrow \Delta T$ |
| FG-2a | $N$，$L$ | | ☆ | | ☆ | $\uparrow Q$ |
| FG-2b | $N$，$L$ | | ☆ | ☆ | | $\downarrow \Delta T$ |
| FG-3 | $N$，$L$ | | | ☆ | ☆ | $\downarrow W$ |
| FN-1 | $N$ | | ☆ | ☆ | ☆ | $\downarrow L$ |
| FN-2 | $N$ | ☆ | | ☆ | ☆ | $\downarrow L$ |
| FN-3 | $N$ | ☆ | | ☆ | ☆ | $\downarrow W$ |
| VG-1 | | ☆ | ☆ | ☆ | ☆ | $\downarrow NL$ |
| VG-2a | $N$，$L$ | ☆ | ☆ | | ☆ | $\uparrow Q$ |
| VG-2b | $N$，$L$ | ☆ | ☆ | ☆ | | $\downarrow \Delta T$ |
| VG-3 | $N$，$L$ | ☆ | | ☆ | ☆ | $\downarrow W$ |

在 FG 法中，傳熱管支數 $N$ 與管長 $L$ 均為固定

在 VG-2與VG-3法則中，$N \times L$ 值為固定

$$h = c_{p,a}\mathrm{Pr}^{-2/3}jG \tag{7-3}$$

由於PEC的比對是以熱傳增強表面(enhanced surface)替換原有的參考表面(referenced surface)，因此吾人有興趣的熱傳特性與原有的參考表面比值如下：

$$\frac{hA}{h_{ref}A_{ref}} = \frac{j}{j_{ref}}\frac{A}{A_{ref}}\frac{G}{G_{ref}} \tag{7-4}$$

同時，推動流體所需要的消耗功率可表示如下：

$$W = \Delta P \times \dot{V} = \left(\frac{fA}{A_c}\frac{G^2}{2\rho}\right)\left(\frac{GA_c}{\rho}\right) \tag{7-5}$$

因此，新的熱傳增強表面與參考表面的耗功比值為：

$$\frac{W}{W_{ref}} = \frac{\left(\frac{fA}{A_c}\frac{G^2}{2\rho}\right)\left(\frac{GA_c}{\rho}\right)}{\left(\frac{f_{ref}A_{ref}}{A_{c,ref}}\frac{G_{ref}^2}{2\rho}\right)\left(\frac{G_{ref}A_{c,ref}}{\rho}\right)} = \frac{f}{f_{ref}}\frac{A}{A_{ref}}\left(\frac{G}{G_{ref}}\right)^3 \tag{7-6}$$

從式7-4與式7-6，可將$G/G_{ref}$消去，因而得到如下的方程式：

$$\frac{\frac{hA}{h_{ref}A_{ref}}}{\left(\frac{W}{W_{ref}}\right)^{1/3}\left(\frac{A}{A_{ref}}\right)^{2/3}} = \frac{\frac{j}{j_{ref}}}{\left(\frac{f}{f_{ref}}\right)^{1/3}} \tag{7-7}$$

# VG-1法則

$Q/Q_{ref}$ 與 $W/W_{ref}$ 是固定的，我們使用新型熱傳增強熱交換器的目的是希望可以適度的減少熱交換器的面積。由 $Q/Q_{ref}$ =1，$hA/h_{ref}A_{ref}$ = 1與 $W/W_{ref}$ = 1，則式7-7可簡化如下：

$$\frac{\frac{hA}{h_{ref}A_{ref}}}{\left(\frac{W}{W_{ref}}\right)^{1/3}\left(\frac{A}{A_{ref}}\right)^{2/3}}=\frac{\frac{j}{j_{ref}}}{\left(\frac{f}{f_{ref}}\right)^{1/3}}\Rightarrow\frac{A}{A_{ref}}=\left(\frac{f}{f_{ref}}\right)^{1/2}\left(\frac{j_{ref}}{j}\right)^{3/2} \quad (7\text{-}8)$$

另外將式7-8代入式7-6可得到：

$$1=\frac{f}{f_{ref}}\frac{A}{A_{ref}}\left(\frac{G}{G_{ref}}\right)^{3}=\frac{f}{f_{ref}}\left(\frac{f}{f_{ref}}\right)^{1/2}\left(\frac{j_{ref}}{j}\right)^{3/2}\left(\frac{G}{G_{ref}}\right)^{3} \quad (7\text{-}9)$$

$$\Rightarrow\frac{G}{G_{ref}}=\left(\frac{j}{j_{ref}}\frac{f_{ref}}{f}\right)^{1/2} \quad (7\text{-}10)$$

# Fundamentals of heat exchanger design, chapter 10

**TABLE 10.6** *Continued*

| Case | Determine: | Information or Constraints Given and Comments | Resultant Formulas to Compute the Objective of the PEC |
|---|---|---|---|
| FG-2b | $\frac{\Delta T_{max}}{\Delta T_{max,p}}$ | $\frac{n_t}{n_{t,p}} = \frac{A_{fr}}{A_{fr,p}} = 1 \quad \frac{L}{L_p} = \frac{A}{A_p} = 1$<br>$\frac{\mathcal{P}}{\mathcal{P}_p} = 1 \qquad \frac{q}{q_p} = 1$ | Compute $UA/(UA)_p$ as outlined for the FG-2a case. Compute NTU from Eq. (10.29) and subsequently, $P$, for the given flow arrangement. Then from Eq. (10.28),<br>$\frac{\Delta T_{max}}{\Delta T_{max,p}} = \frac{P_p}{P}\frac{\dot{m}_p}{\dot{m}}$ |
| FG-3 | $\frac{\mathcal{P}}{\mathcal{P}_p}$ | $\frac{n_t}{n_{t,p}} = \frac{A_{fr}}{A_{fr,p}} = 1 \quad \frac{L}{L_p} = \frac{A}{A_p} = 1$<br>$\frac{q}{q_p} = \frac{\Delta T_{max}}{\Delta T_{max,p}} = 1 \quad \frac{\dot{m}}{\dot{m}_p} = \frac{G}{G_p}$ | From Eqs. (10.26), (10.24), and (10.28)<br>$\frac{UA}{(UA)_p} = \frac{1 + \mathbf{R}_p^*}{(j_p/j)[(f/f_p)(\mathcal{P}_p/\mathcal{P})]^{1/3} + \mathbf{R}^*}$ (1) $\quad \frac{\mathcal{P}}{\mathcal{P}_p} = \frac{f}{f_p}\left(\frac{G}{G_p}\right)^3$ (2)<br>$\frac{q}{q_p} = 1 = \frac{G}{G_p}\frac{P}{P_p}$ (3)<br>From these equations, compute $G/G_p$ as follows: (1) Assume $G/G_p$. (2) Solve for $\mathcal{P}/\mathcal{P}_p$ from Eq. (2). (3) Compute $UA/(UA)_p$ from Eq. (1). (4) Calculate NTU from Eq. (10.28). (5) Determine $P$ and $P_p$ for the exchanger flow arrangement given. (6) compute $q/q_p$ from Eq. (3) which would be different from unity until convergence. Iterate on $G/G_p$ to obtain $q/q_p = 1$. Using converged value of $G/G_p$, calculate $\mathcal{P}/P_p$ from Eq. (2). |
| FN-1 | $\frac{L}{L_p}$ | $\frac{n_t}{n_{t,p}} = \frac{A_{fr}}{A_{fr,p}} = 1 \quad \frac{A}{A_p} = \frac{L}{L_p}$<br>$\frac{\dot{m}}{\dot{m}_p} = \frac{G}{G_p} \quad \frac{\mathcal{P}}{\mathcal{P}_p} = \frac{q}{q_p} = \frac{\Delta T_{max}}{\Delta T_{max,p}} = 1$ | From Eqs. (10.26), (10.24), and (10.28)<br>$\frac{UA}{(UA)_p} = \frac{1 + \mathbf{R}_p^*}{(j_p/j)(f/f_p)^{1/3}(L_p/L)^{2/3} + \mathbf{R}^*(L_p/L)}$<br>$\frac{\mathcal{P}}{\mathcal{P}_p} = 1 = \frac{f}{f_p}\frac{L}{L_p}\left(\frac{G}{G_p}\right)^3, \quad \frac{q}{q_p} = 1 = \frac{G}{G_p}\frac{P}{P_p}$ |

*continued over*

# 其他常見的熱交換器評價方法

熱交換器性能的評價方法相當的多，這些方法可大致歸納如下：

- 直接評價*j*與*f*，作為判別。
- 評價熱傳量與推動流體所需的動力的相互關聯，作為評價基礎。
- 與一參考表面或熱傳管做相對性的評價(如前面介紹的Webb的方法)。
- 其他評價方法(例如Cowell, 1990的方法)。

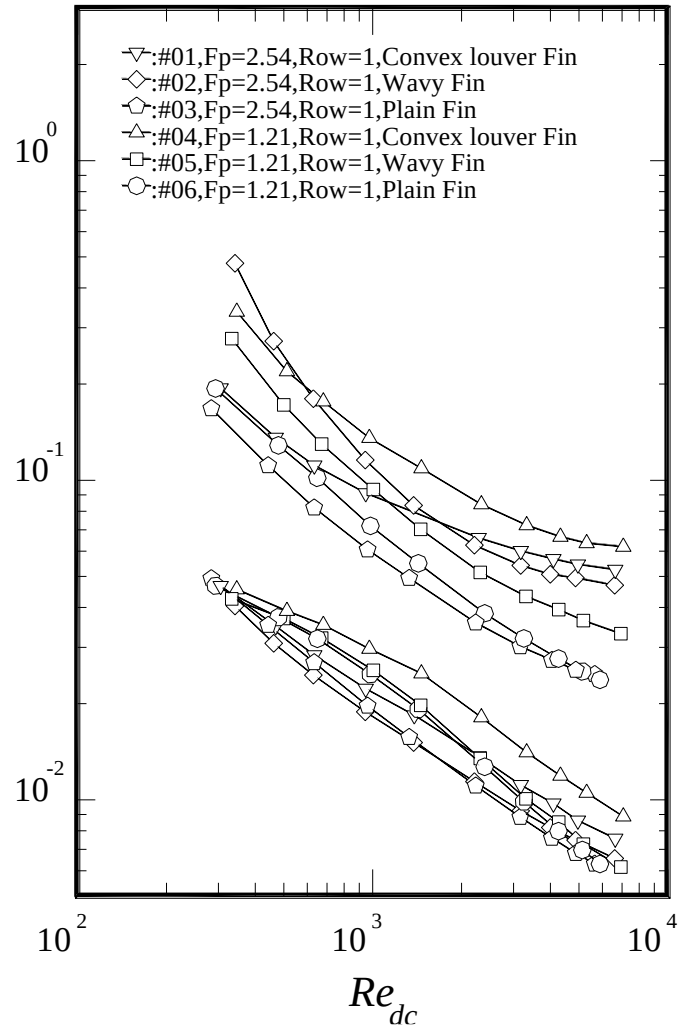


直接熱流特性來評價

# 複合式百葉窗片(convex-louver)、波浪鰭片(wavy)與平板型鰭片(plain)以*j/f*性能指標來評價

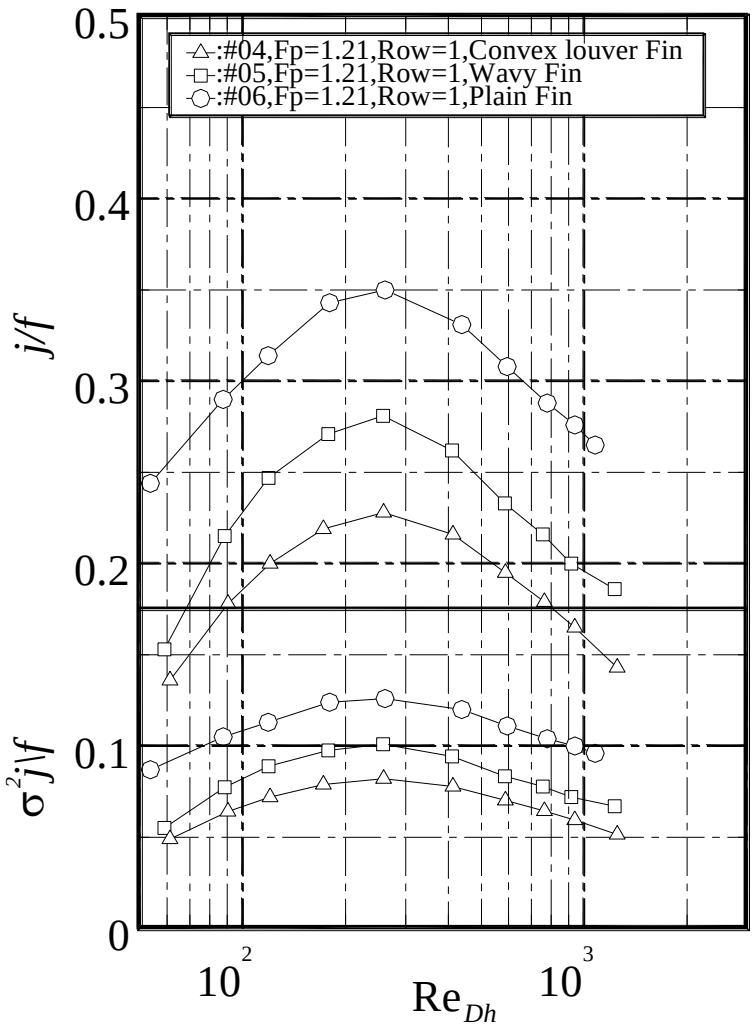


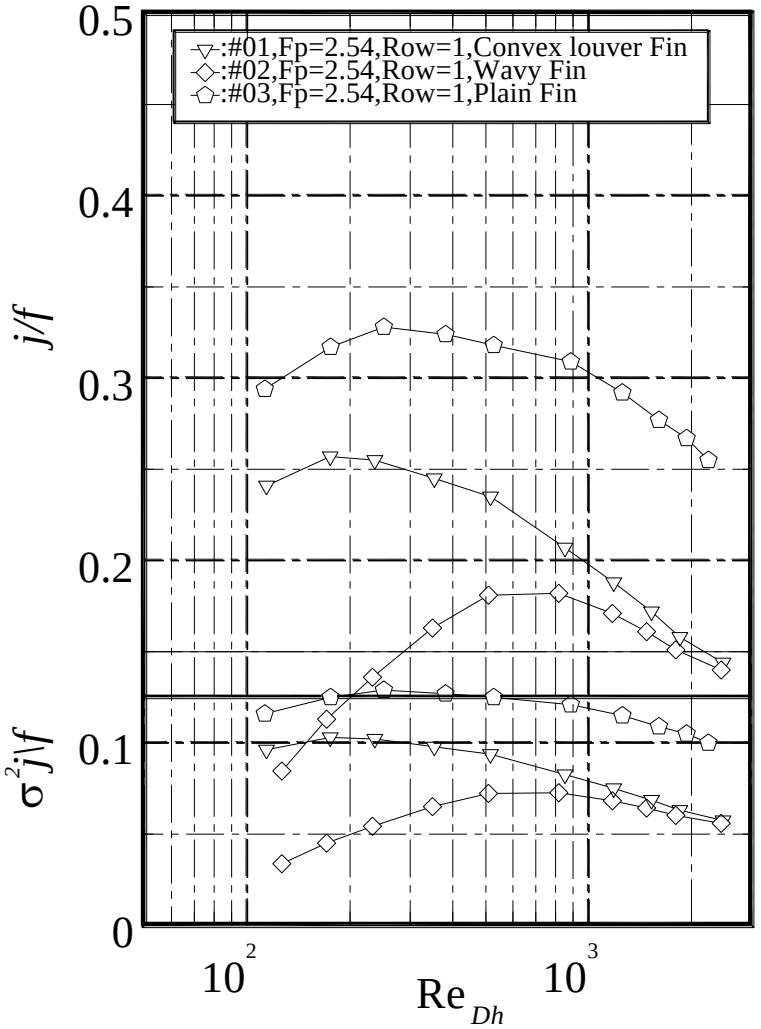

另外一種常用的評價方法為「體積優先」評價法(volume goodness factor comparison, Kays and London ,1950)，採用的評價參數為：

$$\eta_o h_{std}\beta = \frac{c_p \mu}{\mathrm{Pr}^{2/3}} \eta_o \frac{4\sigma}{D_h^2} j\,\mathrm{Re} \qquad (7\text{-}17)$$

$$E_{std}\beta = \frac{\mu^3}{2g_c\rho^2} \frac{4\sigma}{D_h^4} f\,\mathrm{Re}^3 \qquad (7\text{-}18)$$

複合式百葉窗片(convex-louver)、波浪鰭片(wavy)與平板型鰭片(plain) 單位體積、溫差下的熱傳能力與單位體積的摩擦消耗的關係圖

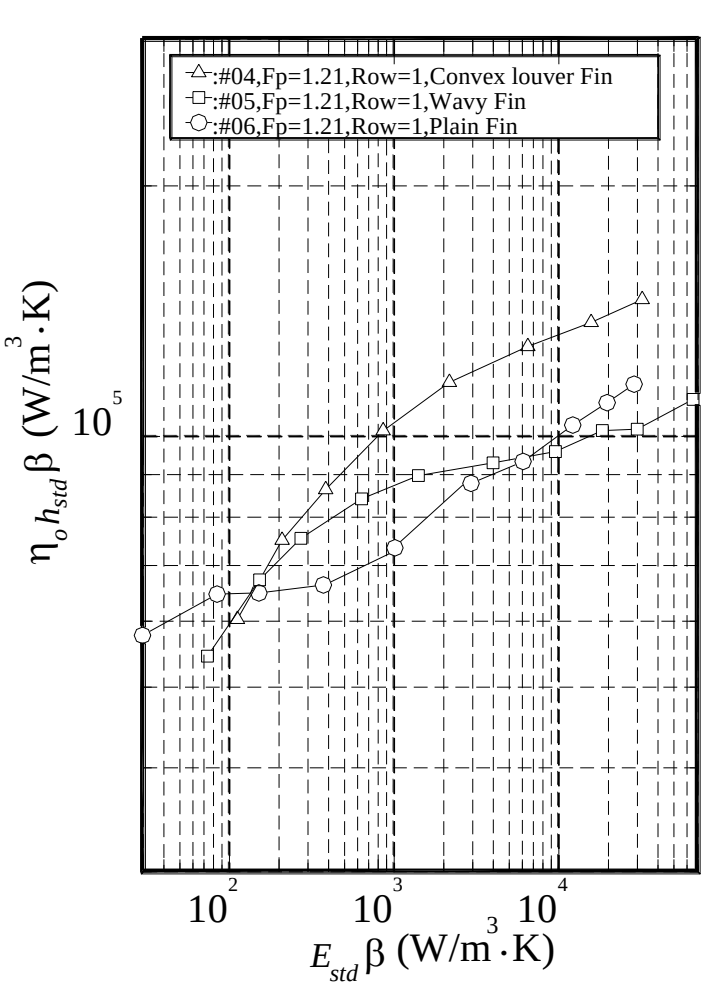


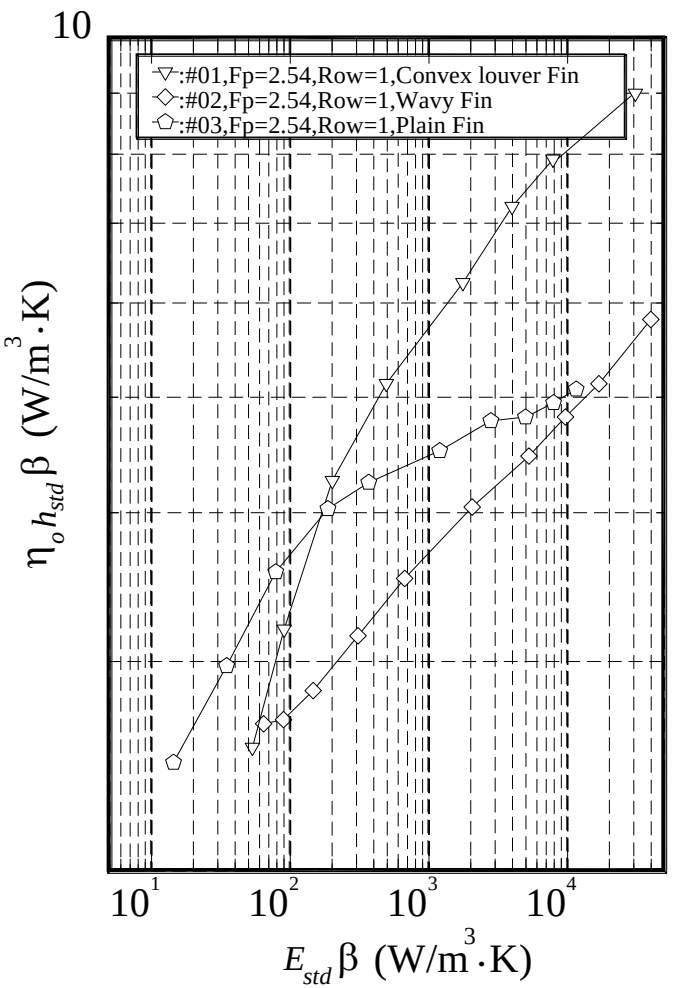

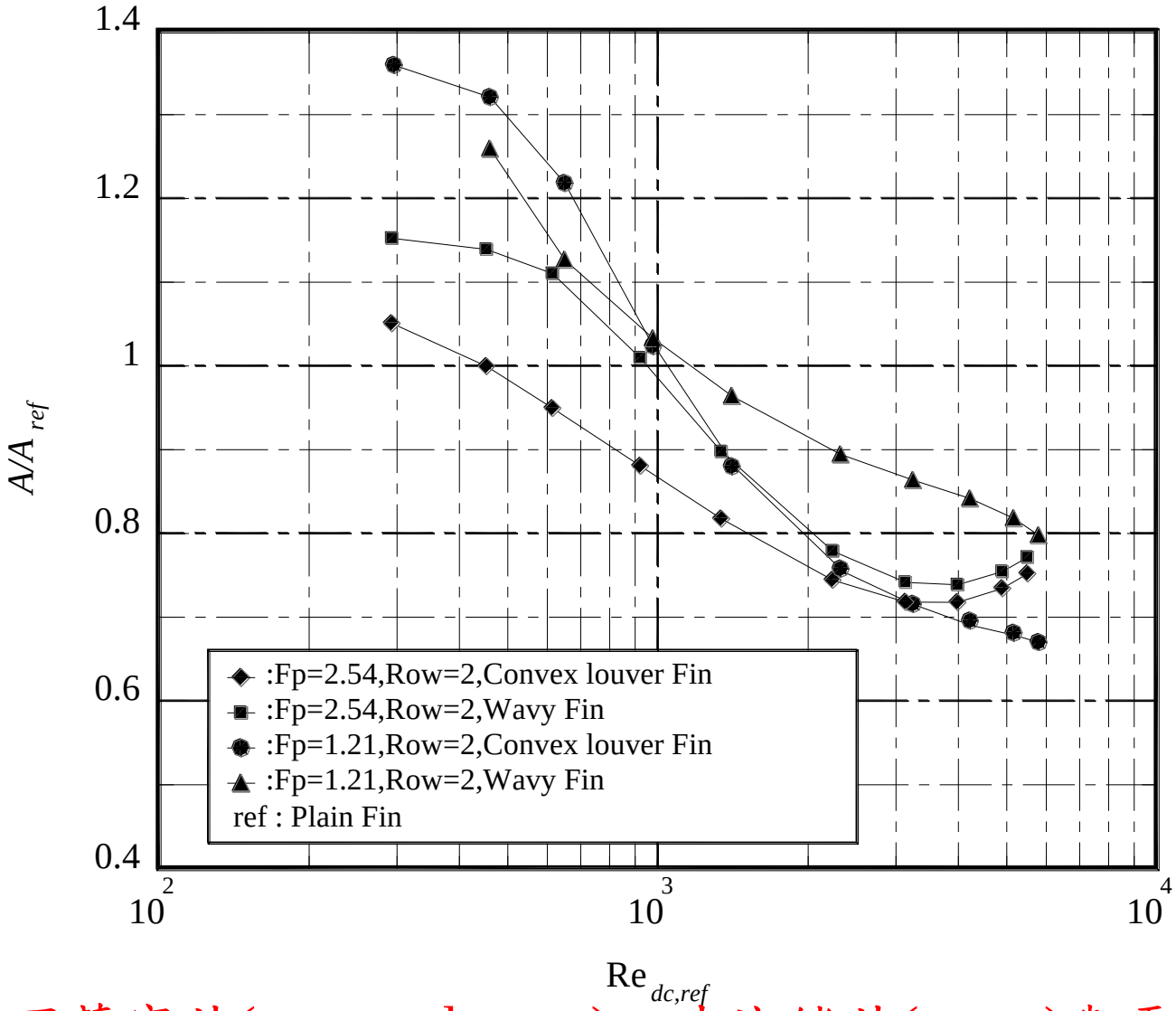


複合式百葉窗片(convex-louver)、波浪鰭片(wavy)與平板型鰭片(plain)以 VG-1法則的性能評價

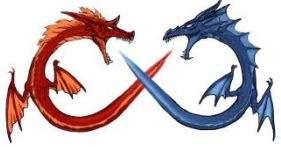

# Classification of enhancement techniques (active methods)

- Mechanical Aids: Examples of the mechanical aids include rotating tube exchangers and scrapped surface heat and mass exchangers.
- Surface vibration.
- Fluid vibration.
- Electrostatic fields.
- Injection.
- Suction.

# Passive enhancement methods..

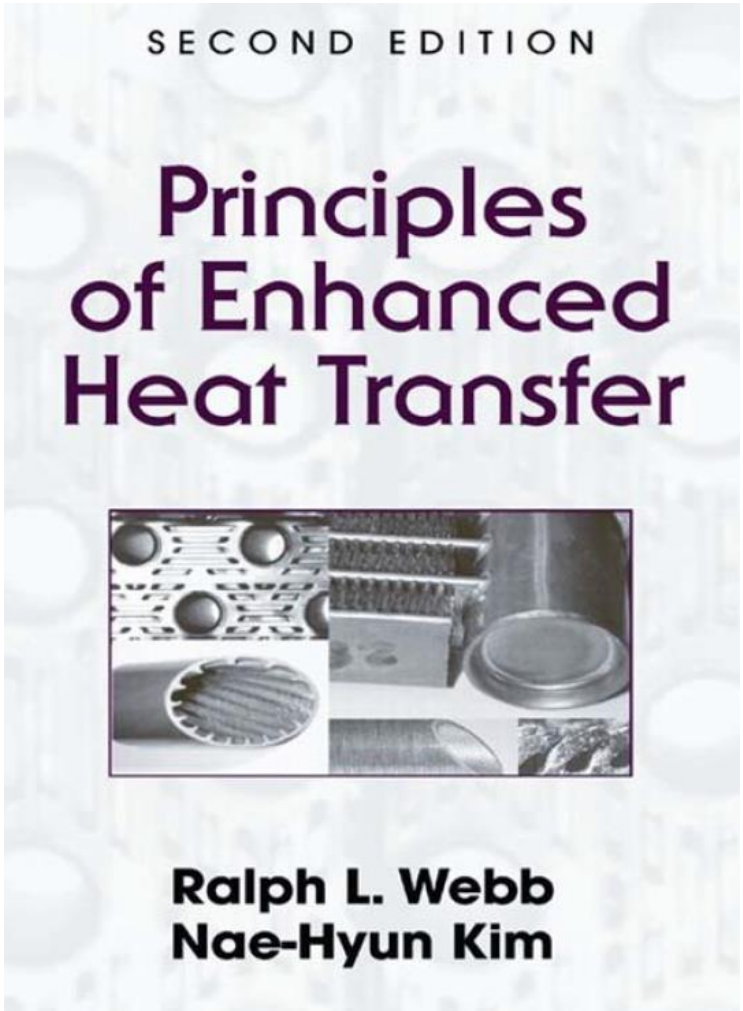


- **Treated Surfaces:** They are heat transfer surfaces that have a fine-scale alteration to their finish or coating. The alteration could be continuous or discontinuous, where the roughness is much smaller than what affects single-phase heat transfer, and they are used primarily for boiling and condensing duties.
- **Rough surfaces:** They are generally surface modifications that promote turbulence in the flow field, primarily in single-phase flows, and do not increase the heat transfer surface area. Their geometric features range from random sand-grain roughness to discrete three-dimensional surface protuberances.
- **Extended surfaces:** They provide effective heat transfer enlargement. The newer developments have led to modified fin surfaces that also tend to improve the heat transfer coefficients by disturbing the flow field in addition to increasing the surface area.
- **Displaced enhancement devices:** These are the insert techniques that are used primarily in confined force convection. These devices improve the energy transfer indirectly at the heat exchange surface by displacing the fluid from the heated or cooled surface of the duct/pipe with bulk fluid to the core flow.
- **Swirl flow devices:** They produce and superimpose swirl flow or secondary recirculation on the axial flow in a channel. These devices include helical strip or cored screw type tube inserts, twisted tapes. They can be used for single phase or two-phase flows heat exchanger.
- **Coiled tubes:** These techniques are suitable for relatively more compact heat exchangers. Coiled tubes produce secondary flows and vortices which promote higher heat transfer coefficient in single phase flow as well as in most boiling regions.
- **Surface tension devices:** These consist of wicking or grooved surfaces, which directly improve the boiling and condensing surface. These devices are most used for heat exchanger occurring phase transformation.
- **Additives for liquids:** These include the addition of solid particles, soluble trace additives and gas bubbles into single phase flows and trace additives which usually depress the surface tension of the liquid for boiling systems.
- **Additives for gases:** These include liquid droplets or solid particles, which are introduced in single-phase gas flows either as dilute phase (gas–solid suspensions) or as dense phase (fluidized beds).

# 熱傳增強管 – 如何使用？

# 層流與紊流之熱傳增強概念

層流

紊流

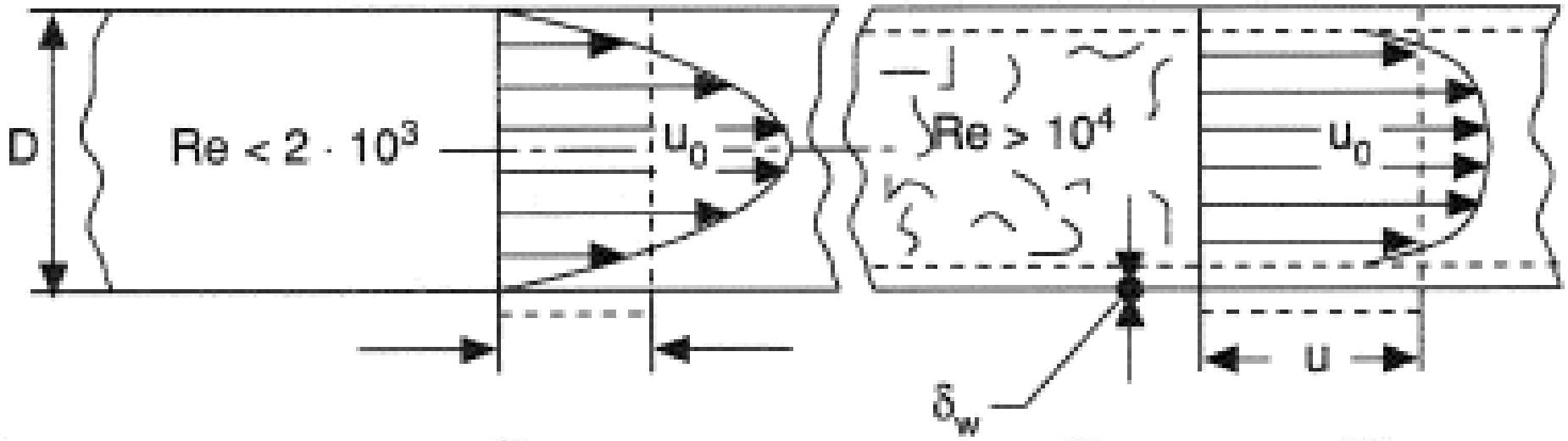


a

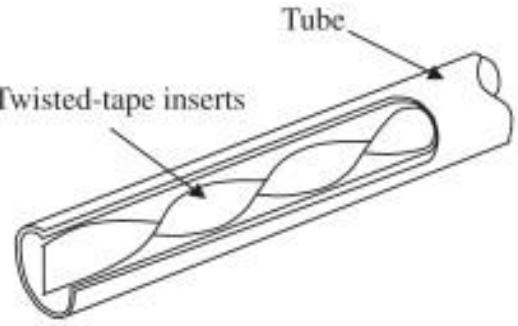


Twisted-tape inserts

b

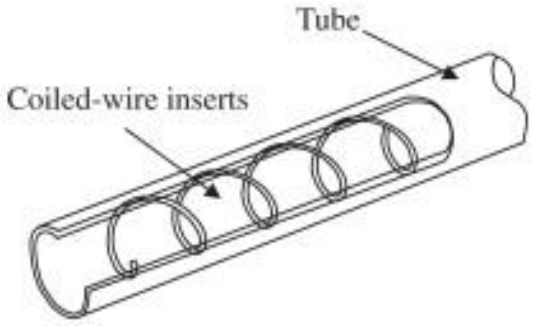


Coiled-wire inserts

c

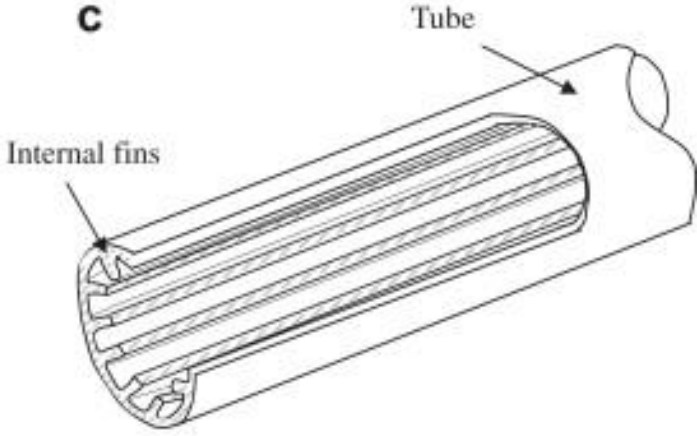


Internal fins

# Review of heat transfer enhancement methods: Focus on passive methods using swirl flow devices, Renewable and Sustainable Energy Reviews 49 (2015 444–469

Fig. 17. Photo of the novel enhanced heat transfer tube [24].

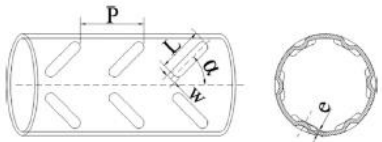


Fig. 19. Structure of the DDIR tube [26].

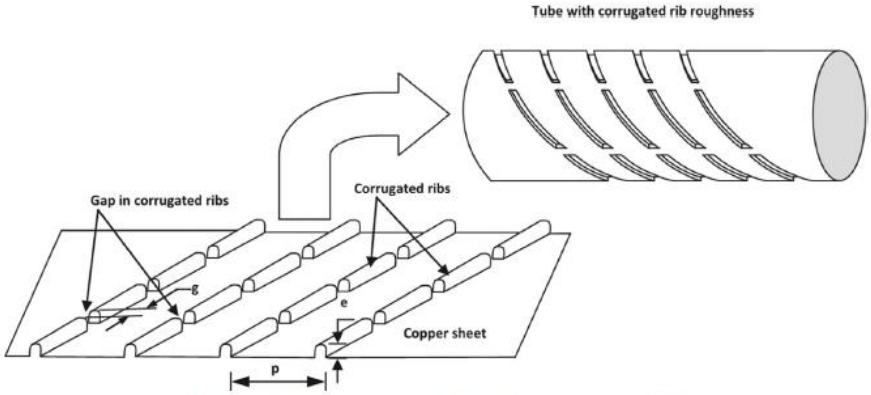


Fig. 18. Typical geometry of circular tube with discrete corrugated ribs [25].

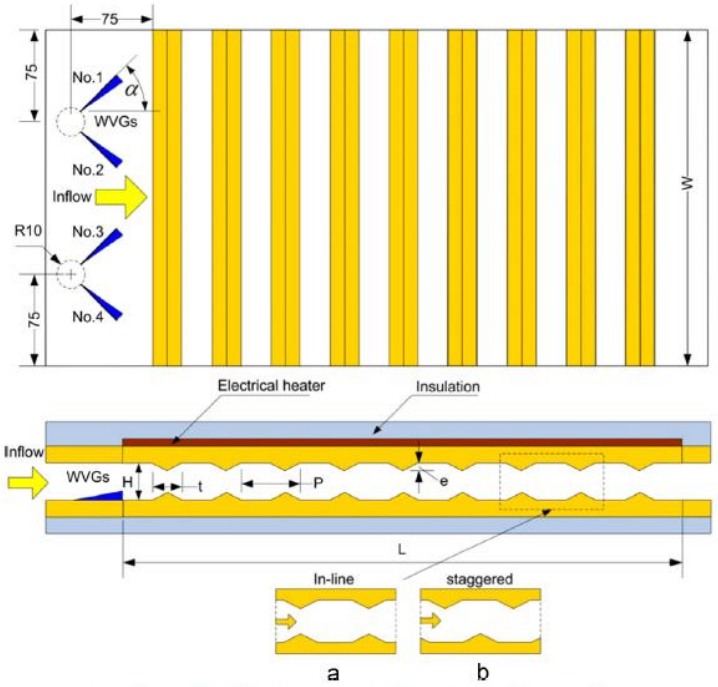


Fig. 20. Test section with WVGs: (a) in-line and (b) staggered rib arrangements [27].


Fig. 15. Helical and transverse corrugated tubes tested [20].

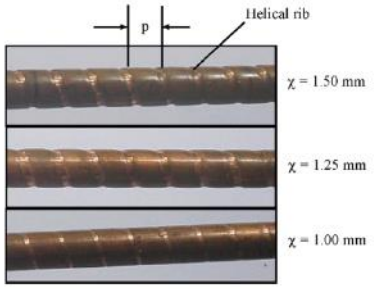


Fig. 16. Photograph of the tube with helical rib used in the present study [23].

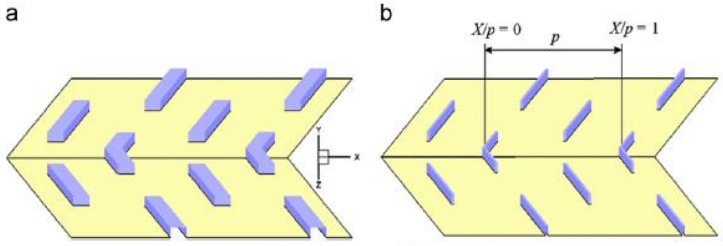


Fig. 21. Arrangement of V-discrete (a) square and (b) thin ribs on lower wall [28].

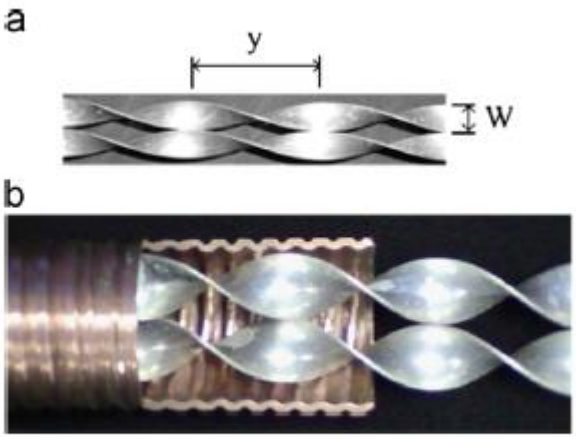


Fig. 30. Details of (a) double twisted tapes and (b) helical-ribbed tube with double twisted tape insert [40].

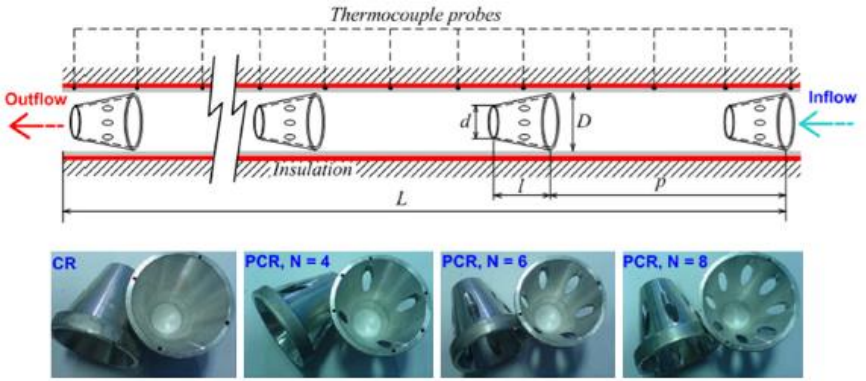


Fig. 40. The arrangement of CR/PCR in a round tube [60].

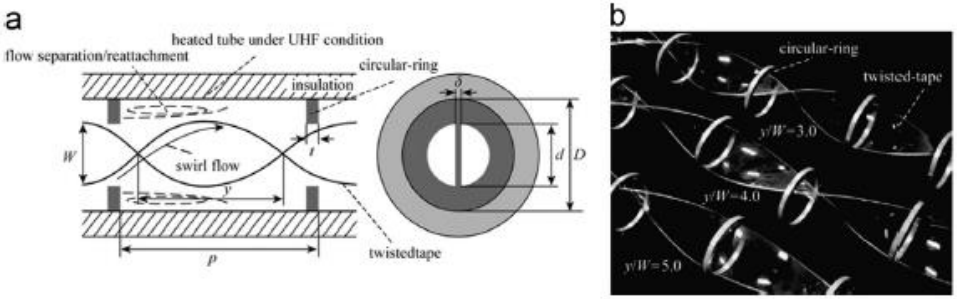


Fig. 45. Diagram and photograph of circular-rings combined with a twisted tape [67].

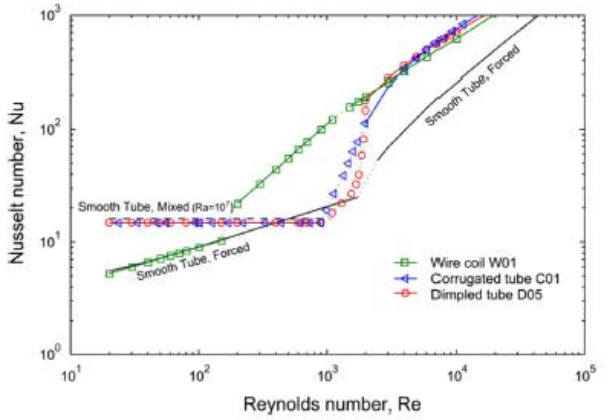


Fig. 48. Nusselt number vs. Reynolds number. Experimental correlations for the wire coil, the corrugated tube and the dim

Full length twisted tape increases the pressure drop comparing to an empty tube. Most of the researches need to reduce the extra pressure drop by using short length twisted tape.Twisted tape in turbulent flow insert is not very effective.

International Communications in Heat and Mass Transfer 74 (2016) 18–26

Contents lists available at ScienceDirect

International Communications in Heat and Mass Transfer

journal homepage: www.elsevier.com/locate/ichmt

# Heat transfer augmentation in a circular tube with perforated double counter twisted tape inserts☆

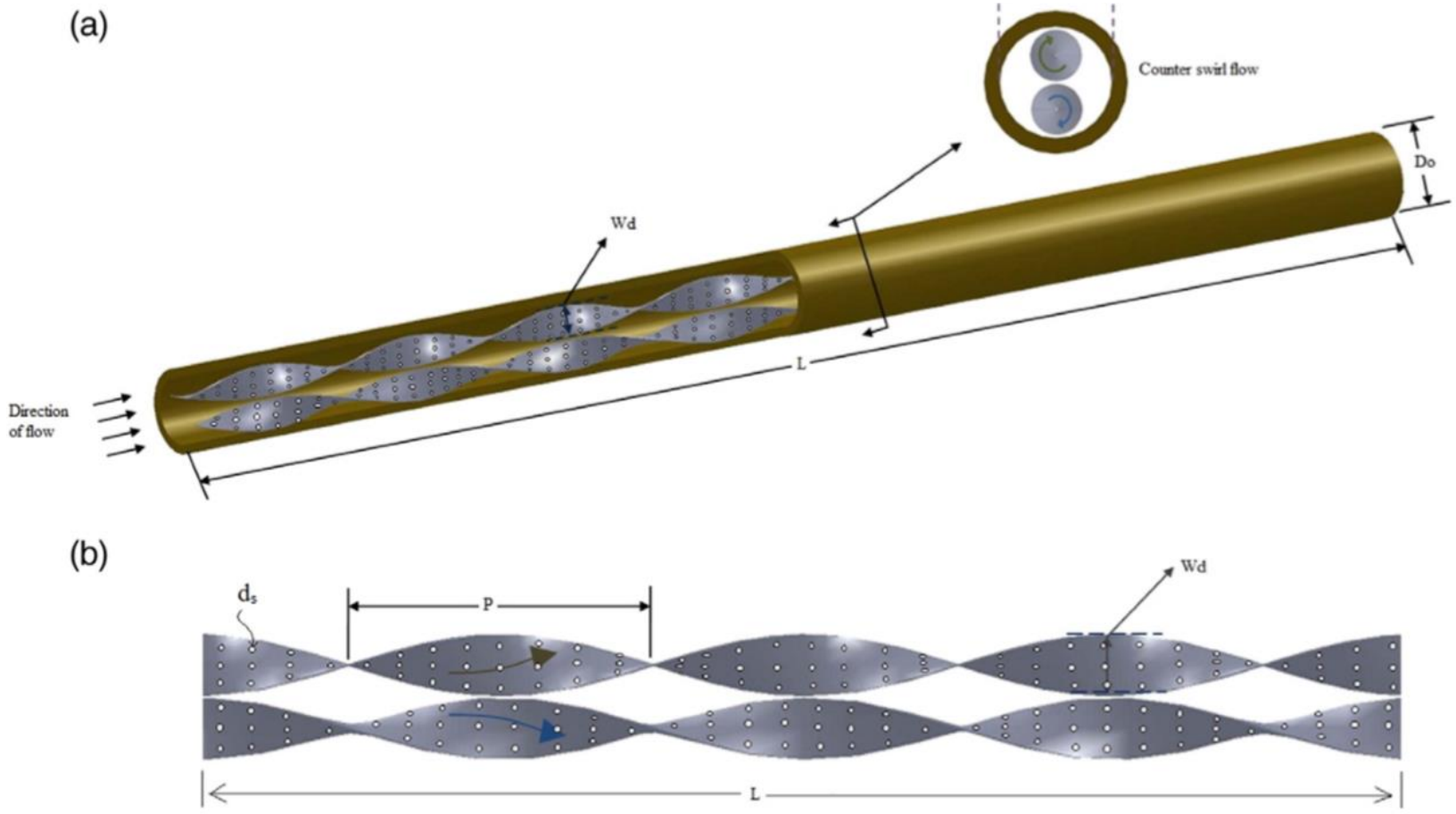


**Fig. 2.** 2(a) Geometry of test section fitted with perforated double counter twisted tape insert; 2(b) Geometric parameters of the perforated double counter twisted tape insert.

A comparative review of self-rotating and stationary twisted tape inserts in heat exchanger, Renewable and Sustainable Energy Reviews, 53(2016)433–449

**Table 2**
Configuration sketches of the stationary twisted tapes.

| Configuration | Name | Reference | Configuration | Name | Reference |
|---|---|---|---|---|---|
| 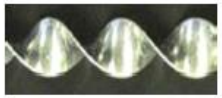 | Typical twisted tape | [34–42] |  | Twisted-tape with V-winglets | [43] |
|  | Perforated twisted tape | [44,45] |  | Left–right twisted tape | [46] |
|  | Notched twisted tape | [47] | 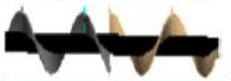 | Right and left helical screw-tape | [48] |
|  | Jagged twisted tape | [47] |  | Helically twisted tape | [49] |
|  | Twisted tape consisting wire nails | [50] |  | Perforated helical twisted-tape | [51] |
| 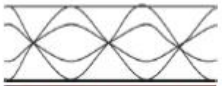 | Center-cleared twisted tape | [52–56] |  | Twisted tape with geometrical progression ratio | [57] |
|  | V-cut twisted tape | [58] |  | Double twisted tape | [59–63] |
|  | Twisted-tape with alternate axes | [64,65] |  | Triple twisted tape | [66] |
|  | Serrated twisted tape | [67] |  | Ribbed spiky twist tape | [68,69] |
|  | Twisted tape consisting of centre wings and alternate-axes | [70] | 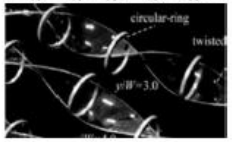  | Twisted tape with circular-rings | [71] |
|  | Peripherally-cut twisted tape with an alternate axis | [72] |  | Staggered twisted tape with central holes | [73] |
| 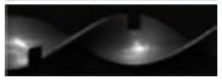 | Square-cut twisted tape | [74–76] |  | Elliptic-cut twisted tape | [77] |
|  | Helical screw tape | [78–80] |  | Regularly-spaced twisted tape | [81] |

Twisted tape with different geometries can offer different performances and mechanisms of heat transfer enhancement. With the purpose of creating stronger turbulence intensity in the vicinity of tube wall or reducing the pressure drop to a required level, slots, holes, cuts, gaps, etc. are manufactured based on the structure of typical twisted tape.

# Twisted tape (types)

## (Usually for single phase applications)

- Typical twisted tape
- Varying length, alternate-axes and pitches twisted tape
- Multiple twisted tapes
- Twisted tape with rod and varying spacer
- Twisted tape with attached fins and baffles
- Twisted tapes with slots, holes, cuts (create more turbulence)
- Helical left–right twisted tape with screw
- Tapes with different surface modifications

A comprehensive review on passive heat transfer enhancements in pipe exchangers, Renewable and Sustainable Energy Reviews 19 (2013) 64–81

**Table 3**
Configuration sketches of various wire coils various.

| Configuration | Name | Reference | Configuration | Name | Reference |
|---|---|---|---|---|---|
|  | Coiled square wires | [40] |  | Twisted tape and wire coil | [42] |
| 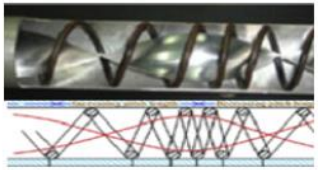 | Non-uniform wire coil combined with twisted tape | [43] |  | Triangle cross sectioned coiled wire | [44] |
| 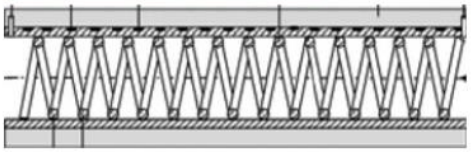 | Coiled wire turbulators | [39] |  | Wire coil in pipe | [46] |

Wire coils is especially for air side (in tube) augmentation

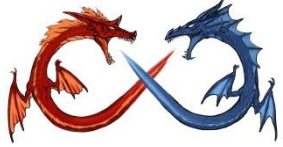

Heat transfer augmentation using twisted tape inserts: A review, Renewable and Sustainable Energy Reviews 63 (2016) 193–225

typical 1-phase enhancement is less than 2

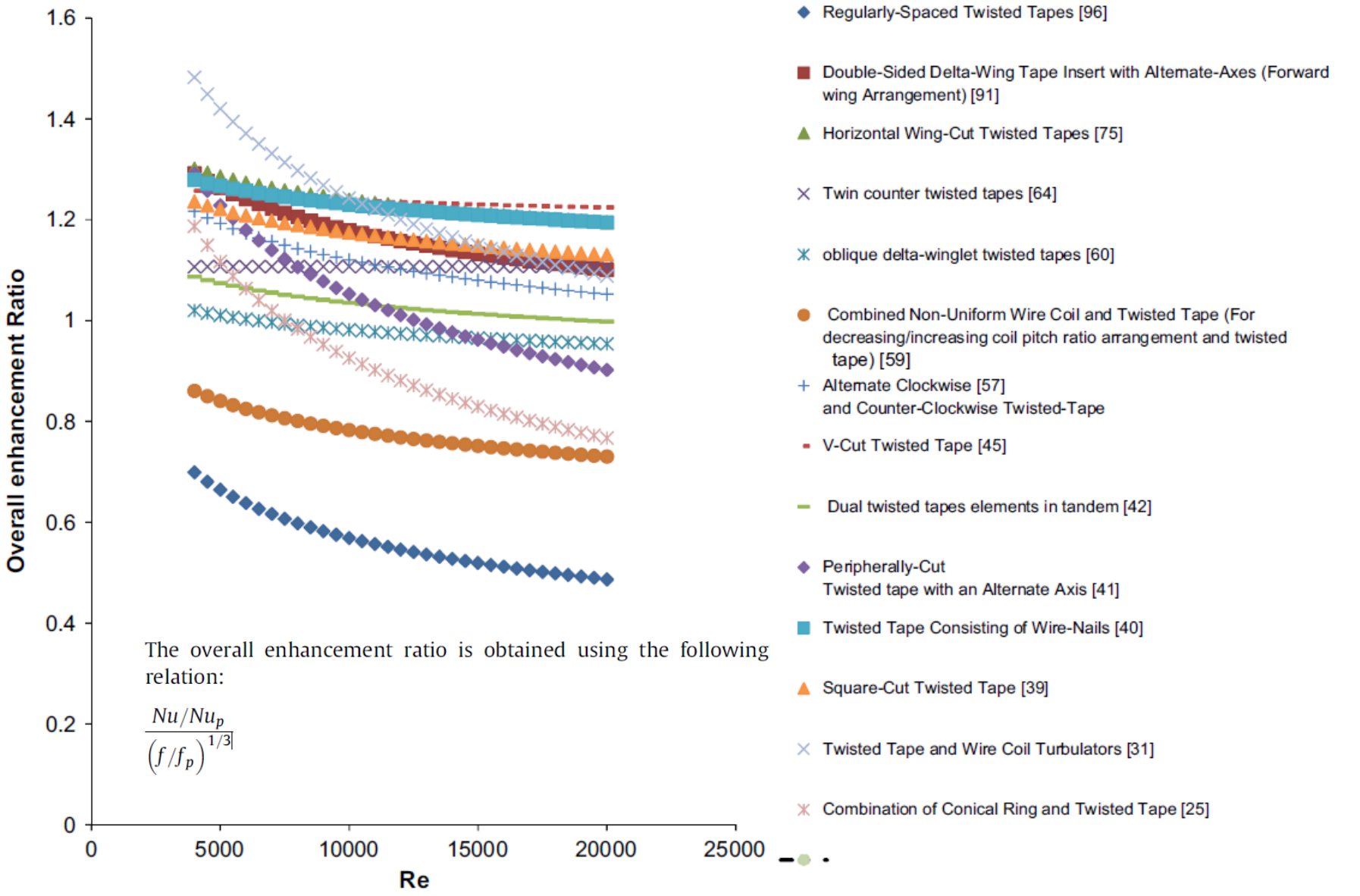


**Fig. 34.** Overall enhancement ratio vs. Reynolds number for different twisted tape geometries.

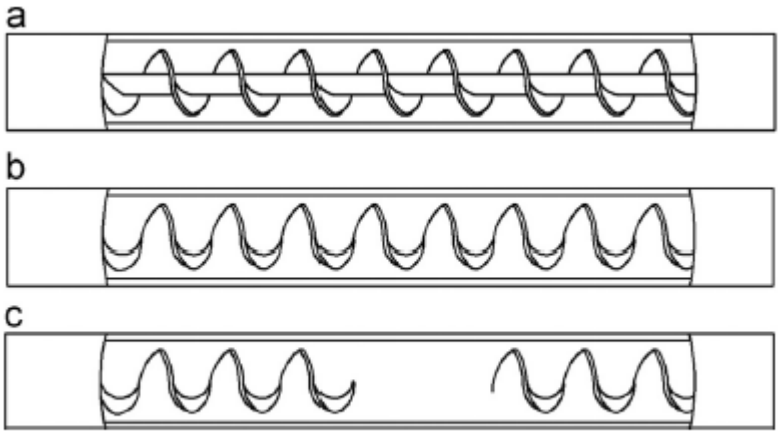


**Fig. 4.** (a) Full length helical tape with a centred rod, (b) full length helical tape without centred rod, (c) regularly spaced helical tapes without rod [17].

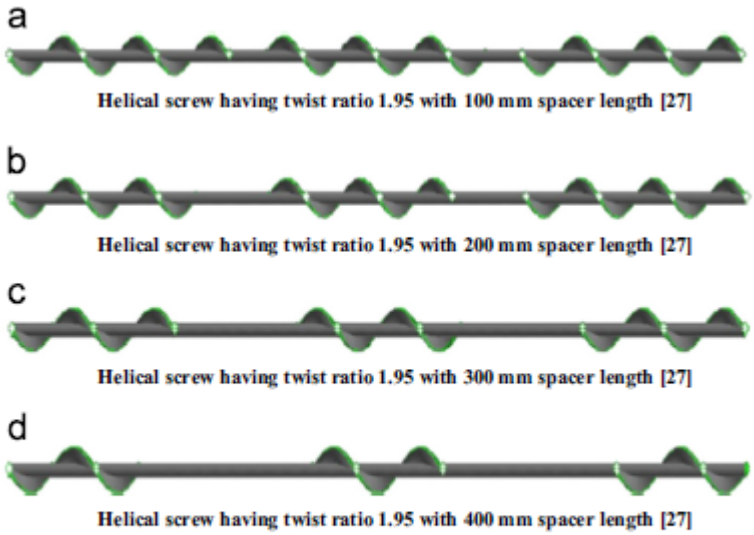


**Fig. 9.** (a) Helical screw having twist ratio 1.95 with 100 mm spacer length [27]. (b) helical screw having twist ratio 1.95 with 200 mm spacer length [27]. (c) helical screw having twist ratio 1.95 with 300 mm spacer length [27]. (d) helical screw having twist ratio 1.95 with 400 mm spacer length [27].

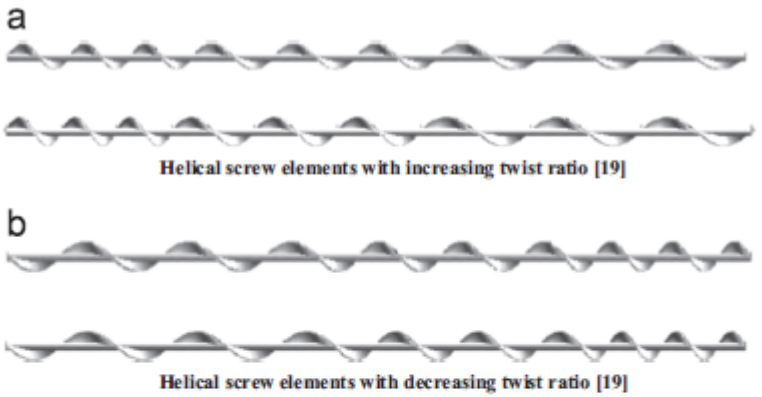


**Fig. 5.** (a) Helical screw elements with increasing twist ratio [19] (b) helical screw elements with decreasing twist ratio [19].

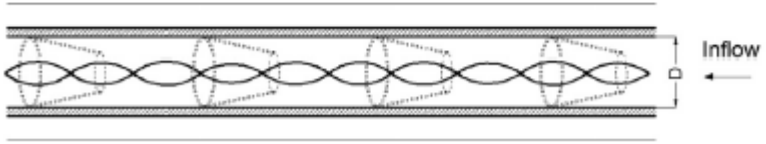


**Fig. 6.** Conical ring turbulator and twisted tape [23].

**Fig. 10.** Tube having twisted tape inserts and wire coil [28].

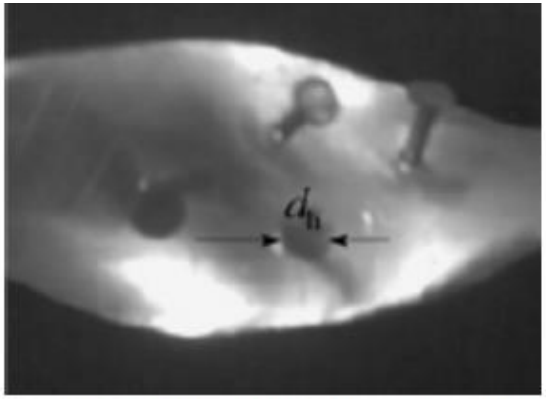


**Fig. 15.** Twisted tape having wire nails studied by Murugesan et al. [36].

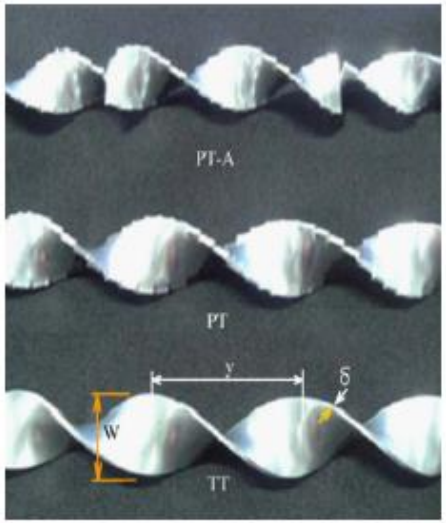


PT-A: Peripherally-cut twisted tapes with alternate axis
PT: Peripherally-cut twisted tapes
TT: Typical twisted tapes
y: Twist length
W: Width of twisted tape
δ: Thickness of twisted tape

**Fig. 16.** Twisted tape studied by Seemawute and Eiasma-ard [37].

**Fig. 22.** rectangular cut twisted tape tested [48].

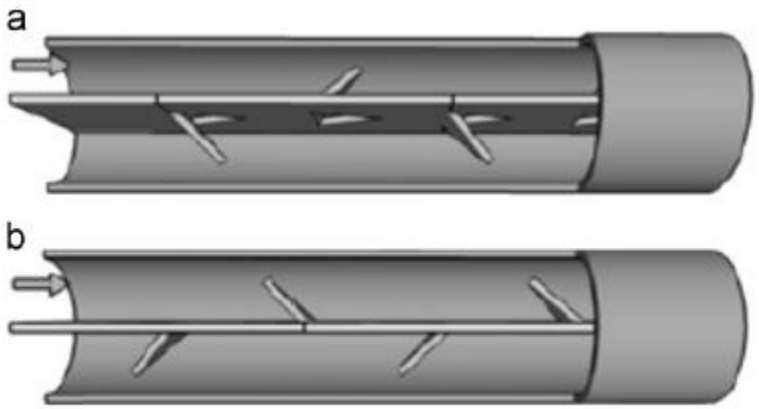


**Fig. 31.** (a) Backward wing arrangement (b) Forward wing arrangement (Eiamsa-ard and Promvonge [87]).


**Fig. 24.** Decreasing/increasing coil pitch ratio arrangement and twisted tape [54].

**Fig. 18.** Perforated twisted tapes with parallel wings [40].

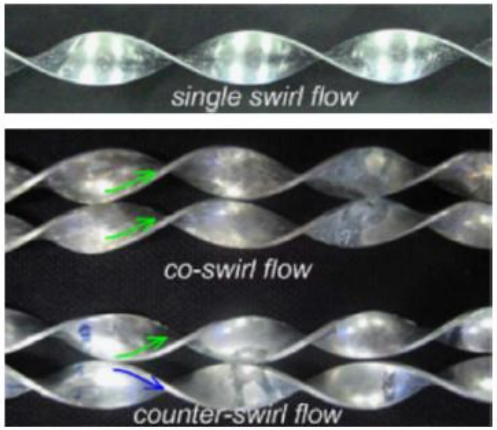


**Fig. 25.** Single twisted tape (single swirl flow), twin co-twisted tape (co swirl flow) and twin counter twisted tapes (counter-swirl flow) [59].

$$\eta = \frac{Nu_T/Nu_0}{(f_T/f_0)^{1/3}}$$

**Table 1**
Configuration sketches of the self-rotating twisted tapes.

| Configuration | Illustration | Name | Reference |
|---|---|---|---|
| 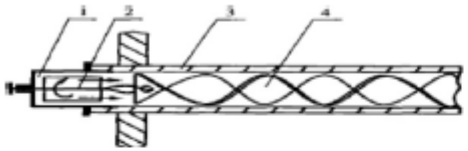 | 1 – Tube bearing, 2 – spindle, 3 – tube, 4 – twisted tape | Typical twisted tape | [14–21] |
| 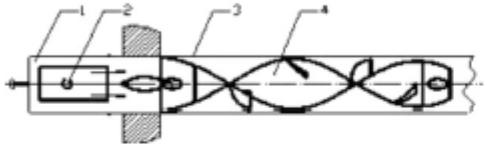 | 1 – Tube bearing, 2 – spindle, 3 – tube, 4 – twisted tape with oblique teeth | Oblique teeth twisted tape | [22] |
| 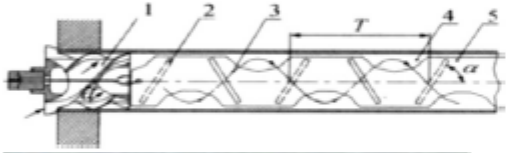 | 1 – Tube bearing, 2 – straight strip with elliptical teeth and broken edge, 3 – spiral line, 4 – elliptical teeth, 5 – straight strip | Straight strip with elliptical teeth and broken edge | [23] |
|  | – | Miniature hydraulic turbine | [24–28] |
|  | – | Triangular groove twisted tape | [29,30] |
|  | – | Semicircle groove twisted tape | [31] |
|  | – | Regularly spaced twisted tape | [32] |
|  | – | Helically twisted tape | [33] |

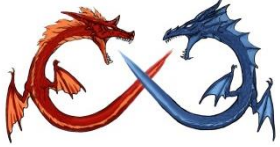

# Stationary vs. self rotating twisted tape

- The stationary twisted tapes can generate the swirl flow in the fluid flow, which can enhance the flow turbulence intensity, and lead to better convection heat transfer compared to the plain tube with an axial flow.
- The self-rotating twisted tapes can strengthen the heat transfer efficiency and achieve on-line automatic anti-scaling and descaling effect.
- The self-rotating twisted tapes change the direction of fluid flow, form a rotational flow, get the bulk flow and fluid at the tube surface mixed and disrupt the development of boundary layer. Compared with the stationary twisted tapes, the self-rotating twisted tapes have the dual effects (swirled and mixing).

# 典型沸騰(蒸發)管

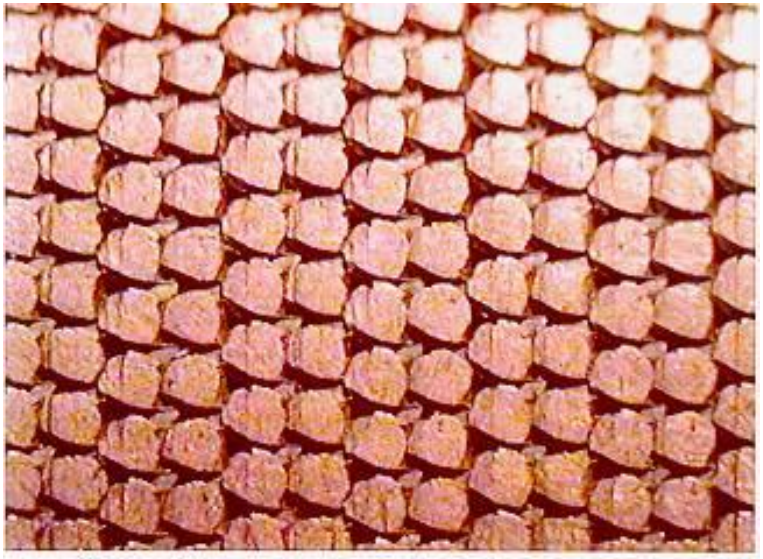

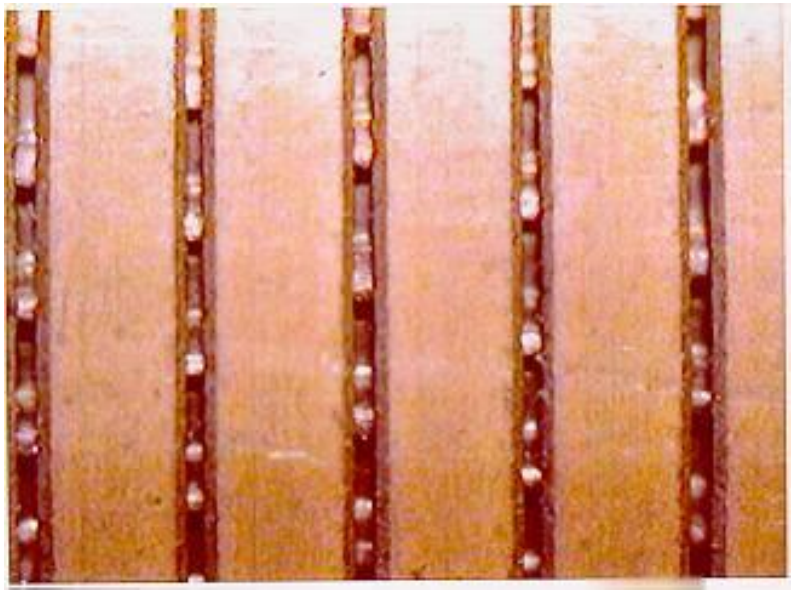

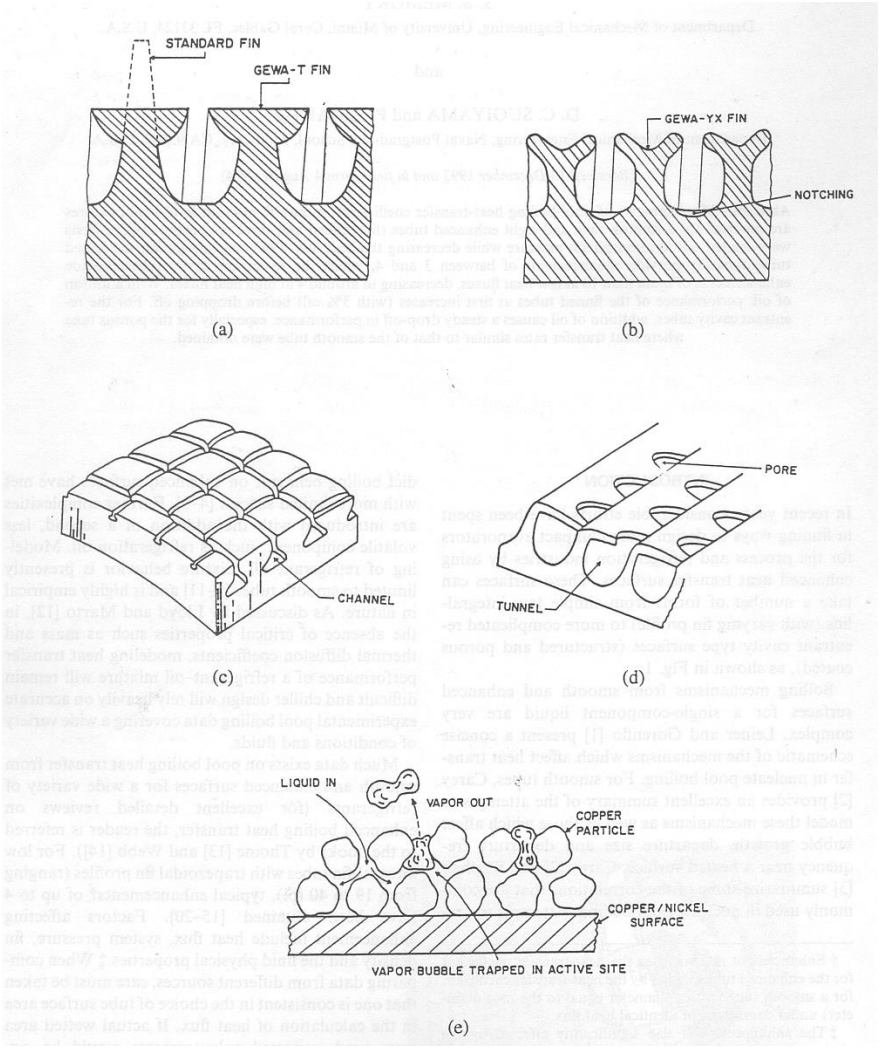
STANDARD FIN
GEWA-T FIN
(a)
GEWA-YX FIN
NOTCHING
(b)
CHANNEL
(c)
PORE
TUNNEL
(d)
LIQUID IN
VAPOR OUT
COPPER PARTICLE
COPPER/NICKEL SURFACE
VAPOR BUBBLE TRAPPED IN ACTIVE SITE
(e)

# 典型蒸發與冷凝管

Shell side boiling

Shell side condensation

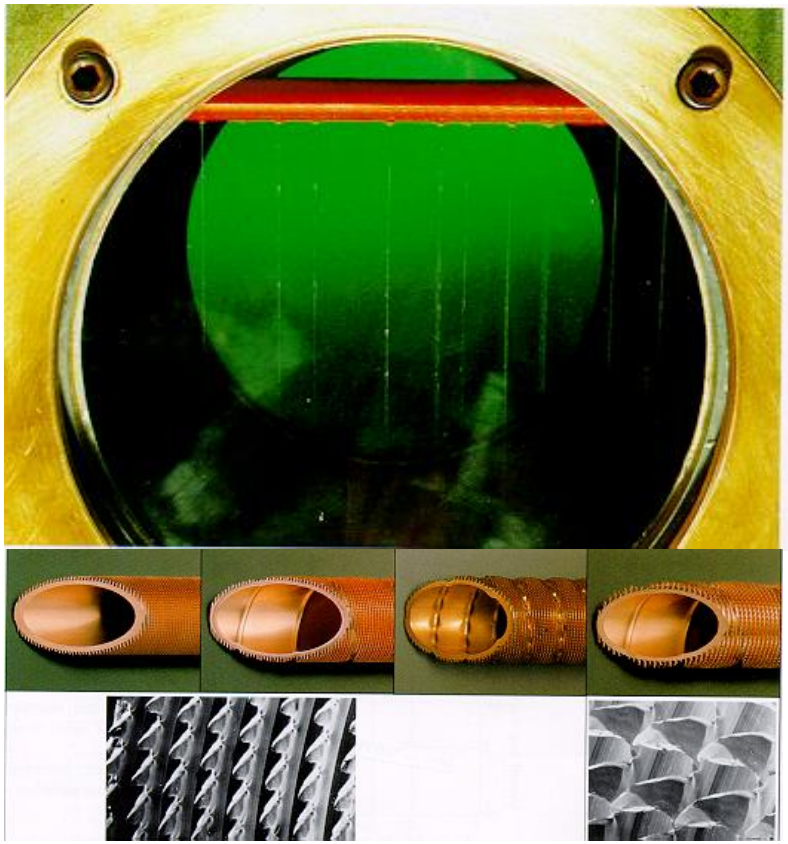

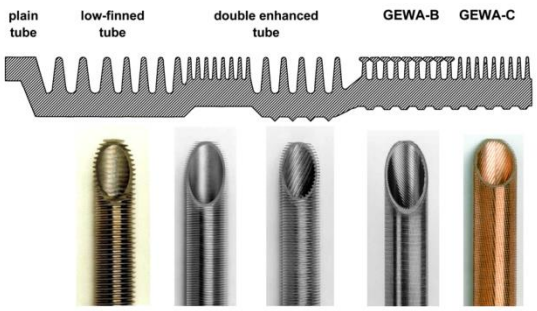


Fig. 3 – Low-finned and double enhanced tubes.

Copyright © Taylor and Francis Group, LLC
ISSN: 0145-7632 print / 1521-0537 online
DOI: 10.1080/01457632.2014.939527

# Heat Transfer Performance of an Edge-Shaped Finned Tube

5-7 times increase in HTC while only 2-3 times increase of HTC for typical low fin tube

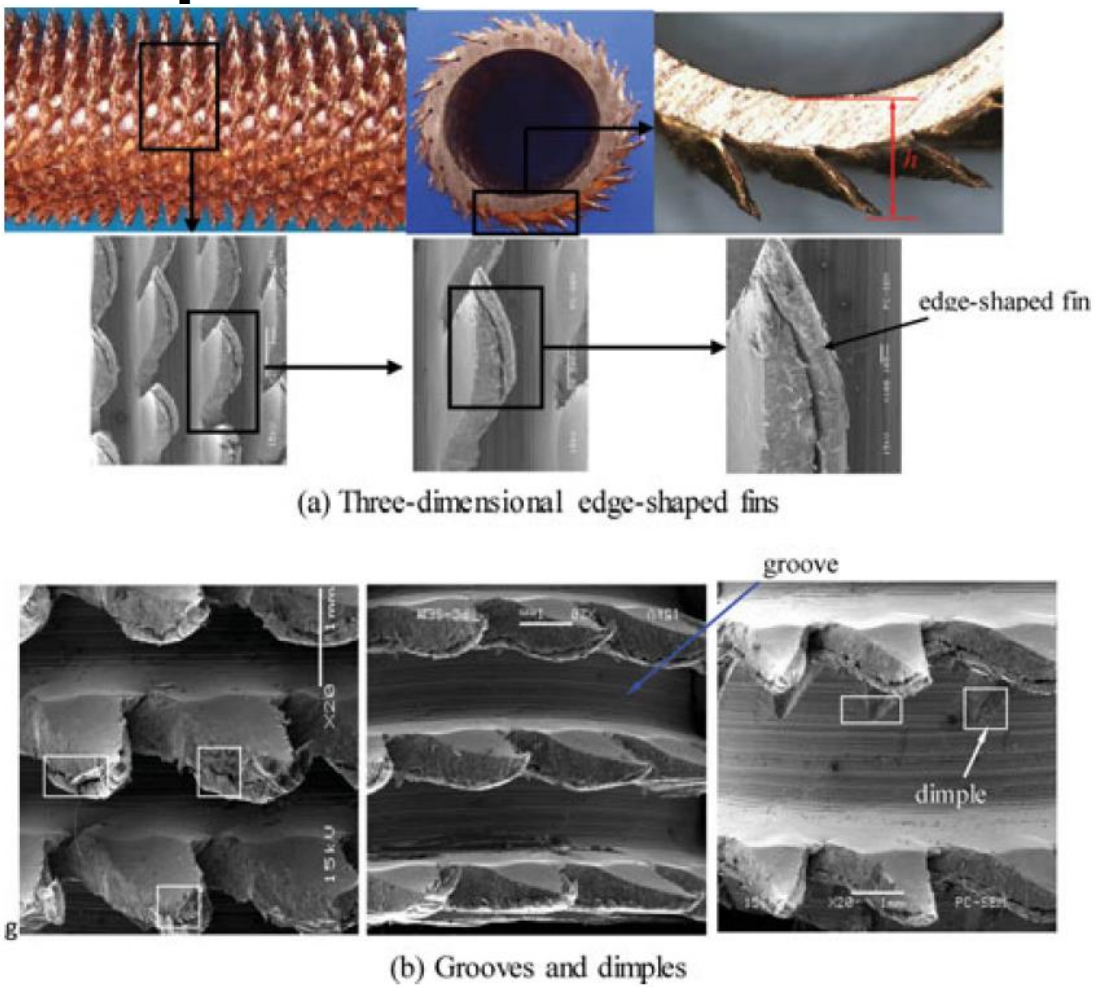


(a) Three-dimensional edge-shaped fins

(b) Grooves and dimples

**Figure 1** Fins, grooves, and dimples on the tube fabricated by ploughing–extruding process: (a) three-dimensional edge-shaped fins, and (b) grooves and dimples.

# Using swirled baffle to improve 殼管式熱交換器 (Shell-and-tube HX)

- Typical Shell and tube HX
  - 殼管式熱交換器不是非常的密集 (non-compact)。
  - 在外型上，殼管式熱交換器的設計非常的「強壯」，因此非常適用於高壓的應用上。
  - 可廣泛地適用於不同的應用場合，例如惡劣的工作環境與特殊的工作流體。
  - 可適用高溫與高壓的應用場合。

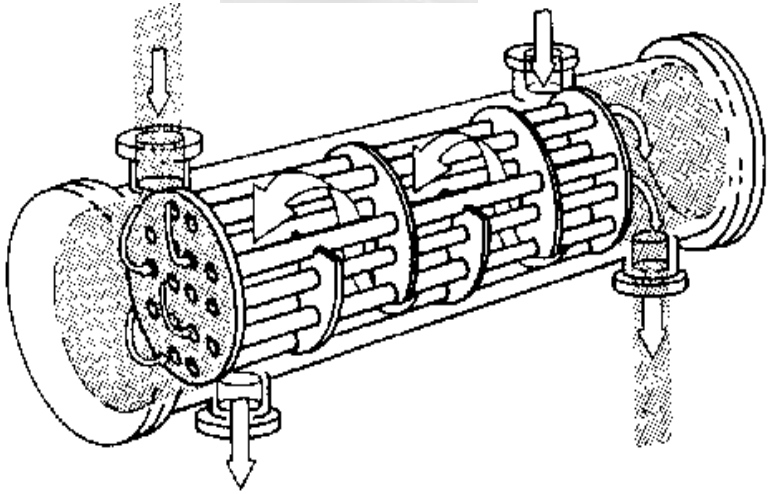

# 傳統式阻流板流場示意圖

流體以180°轉折方式前進

阻流板

轉折處會出現大量漩渦造成熱傳效率差、積垢與沉積腐蝕

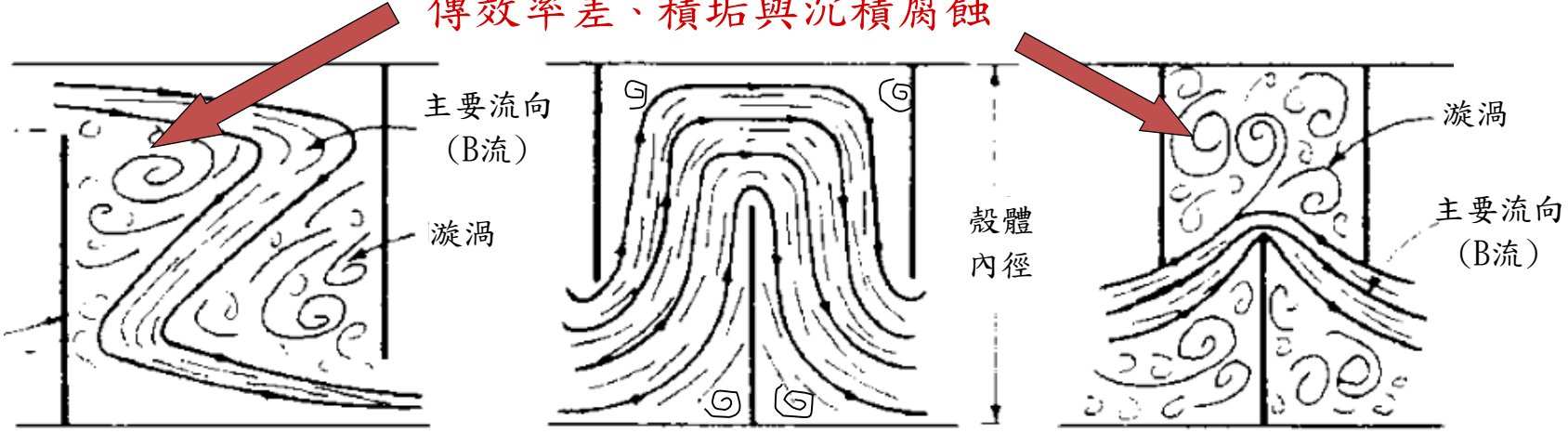


開口率小　開口率適中　開口率大

# 傳統殼管式的缺點

- 殼側高壓損 (due to the sudden contraction and expansion of flow, and fluid impinging on the shell wall caused by segmental baffles)，需要較大的Pump與操作功耗
- 較低的熱傳性能 (due to the flow stagnation in the so-called “stagnation regions,”)
- 較低的殼側流速 (due to the leakage between baffles and shell wall caused by inaccuracy in manufacturing tolerance and installation)
- 管群的流動震盪(due to the vibration caused by shell-side flow normal to tube bundle)

# Enhancement via directing..
# HELIXCHANGER® 的優點與效益

降低殼側積垢速率與
增加操作時間3~4倍

**平均可節省**
**整體成本**
**20%**

減少所需
熱傳面積最
高35%

減少設備
停車保養
時間

製程流量負
荷提升最高
40%

可降低殼側
壓降值，減少
PUMP系統成本

可避免傳熱管
共振損壞

- **Lummus**獨家專利技術
- 專利名： **HELIXCHANGER®**

US 20080190593A1

(19) United States

(12) Patent Application Publication

Wang et al.

(10) Pub. No.: US 2008/0190593 A1

(43) Pub. Date: Aug. 14, 2008

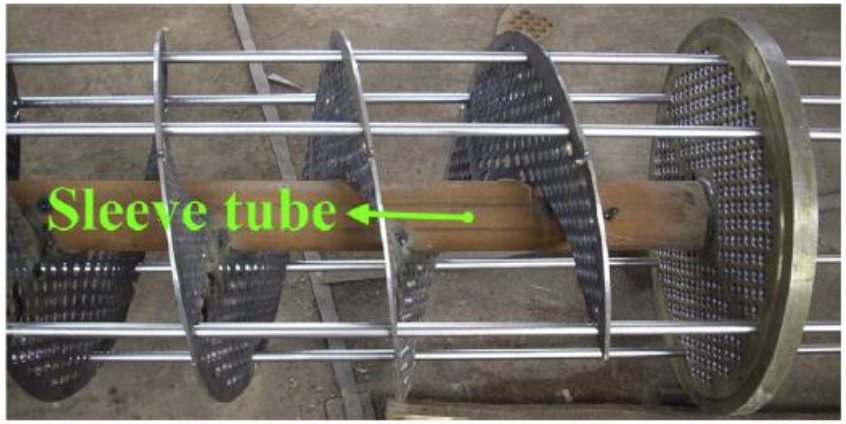


Fig. 1. Central sleeve tube of a continuous helical baffled STHX [30].

# Continuous Helix baffle

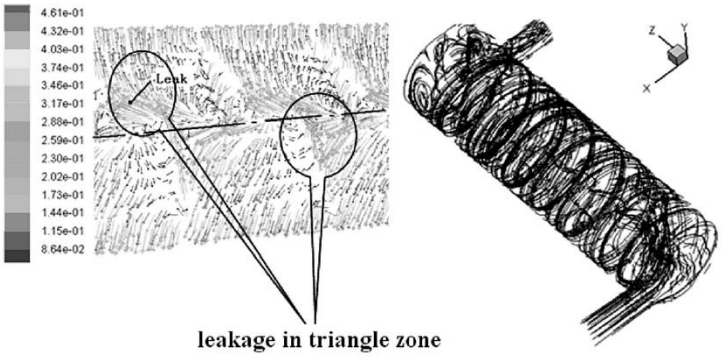


**Figure 8** Flow field in symmetrical interface of heat exchangers with overlap helical baffles [32].

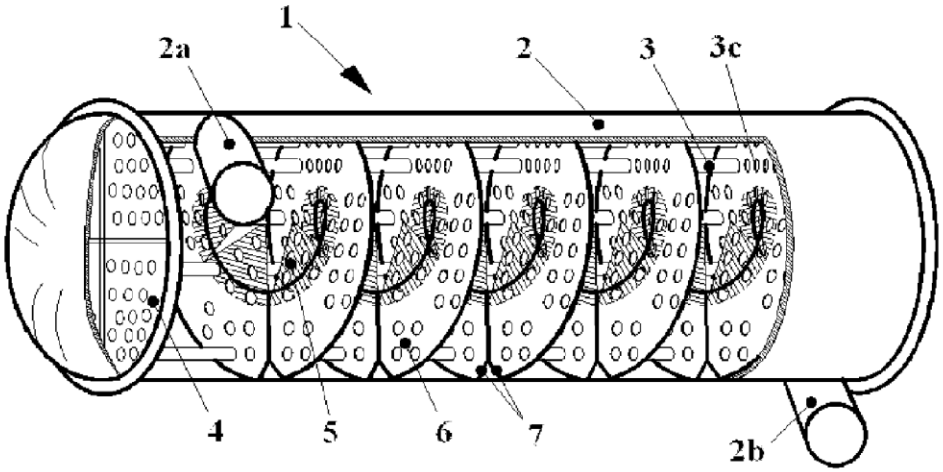

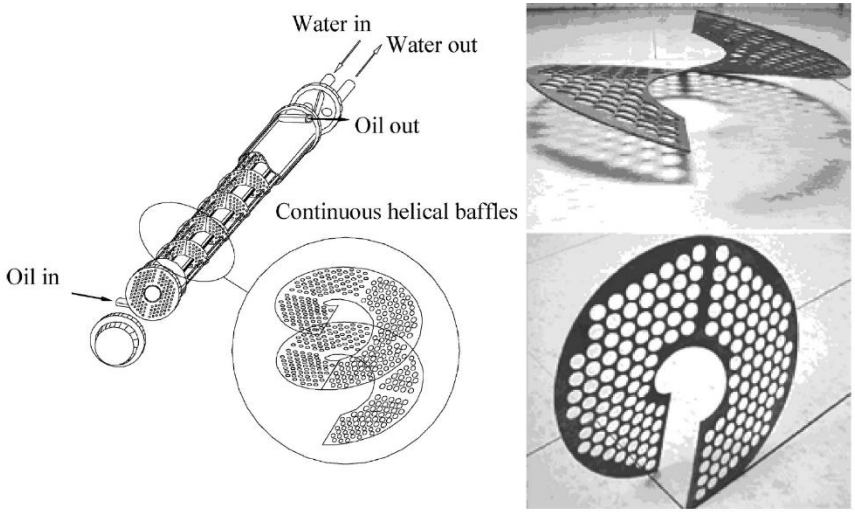


**Figure 10** Heat exchanger with continuous helical baffles [44].

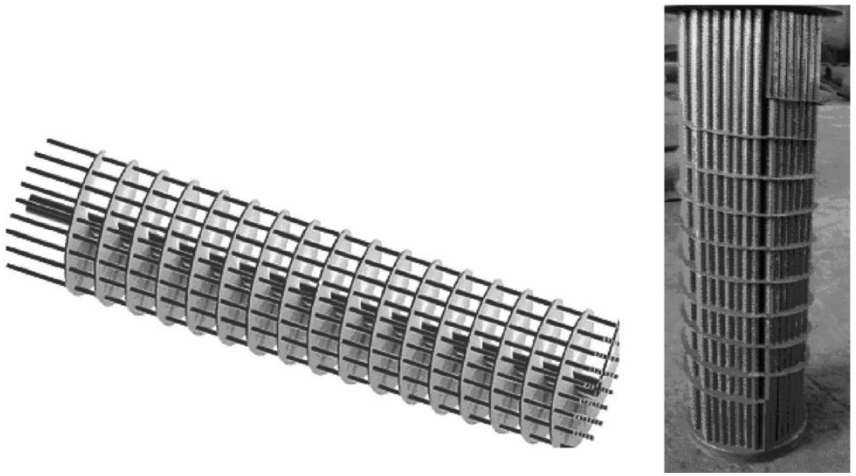

**Figure 11** Tube bundle of STHX with continuous helical baffles [45].

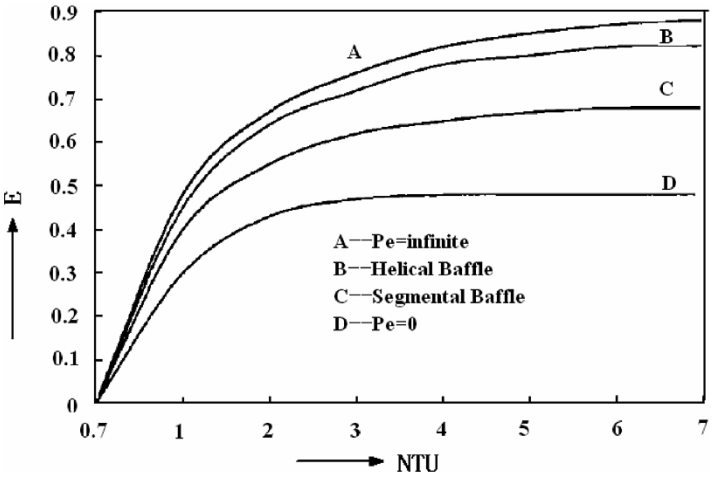


**Figure 4** Heat exchanger effectiveness for segmental baffles and helical baffles [17].

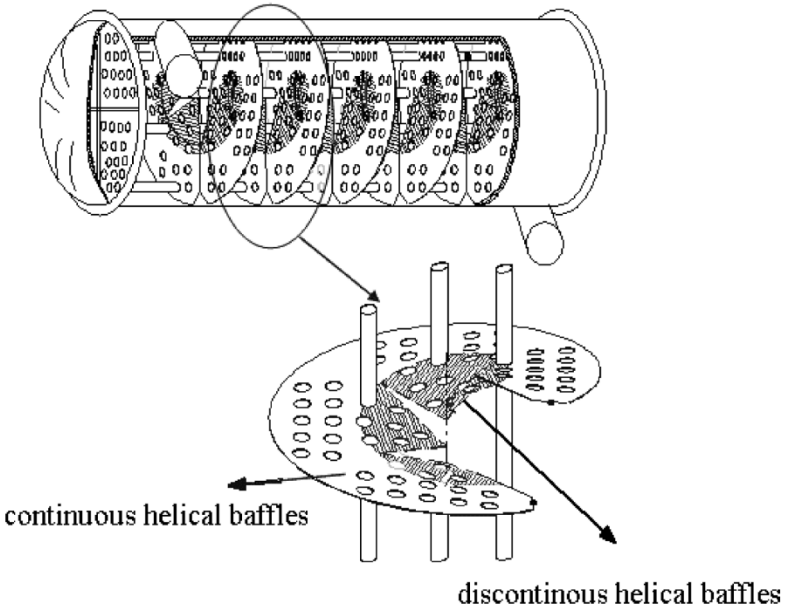


**Figure 16** Schematic of combined single shell-pass heat exchangers with helical baffles [54].

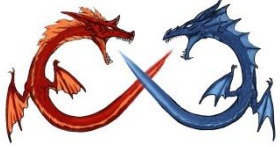

*Heat Transfer Engineering*, 31(10):836–853, 2010
Copyright © Taylor and Francis Group, LLC
ISSN: 0145-7632 print / 1521-0537 online
DOI: 10.1080/01457630903547602

Taylor & Francis
Taylor & Francis Group

# Review of Improvements on Shell-and-Tube Heat Exchangers With Helical Baffles

QIUWANG WANG, GUIDONG CHEN, QIUYANG CHEN, and MIN ZENG

**Table 6** Main characteristics of shell-and-tube heat exchangers for preheating crude oil [5, 17]

| | Shell-and-tube heat exchangers with | | | |
|---|---|---|---|---|
| | Segmental baffles | | Helical baffles (40°) | |
| Characteristic | Tube side | Shell side | Tube side | Shell side |
| Process fluid | Kerosene | Crude oil | Kerosene | Crude oil |
| Mass flow rate (kg/h) | 2.8 | 25 | 2.8 | 25 |
| Inlet temperature (°C) | 200.7 | 10 | 200.7 | 10 |
| Outlet temperature (°C) | 46.5 | 32.1 | 46.5 | 32.1 |
| Dynamic viscosity (Pa-s) | 0.61011e-3 | 6.96288 e-3 | 0.6066e-3 | 6.9841 e-3 |
| Shell diameter (mm) | 491 | | 491 | |
| Tubes | | | | |
| OD (mm) | 20 | | 20 | |
| Length (mm) | 3,985 | | 4,171 | |
| Number | 220 | | 220 | |
| Number of passes | 4 | 1 | 4 | 1 |
| Heat duty (kW) | 1,015.8 | | 1,006.4 | |
| Area ( $m^2$) | 55.08 | | 57.66 | |
| HTC ($W/m^2$-K) | 448.21 | 997.15 | 452.02 | 729.7 |
| Pressure drop (kPa) | 2.52 | 43.55 | 2.6 | 17 |
| Capital cost | | | | |
| $ | 45,522 | | 46,251 | |
| $/yr | 8,116 | | 8,246 | |
| Operation cost ($/yr) | 1,189 | | 470 | |
| Total cost ( $/yr) | 9,305 | | 8,716 | |

**Table 2** Compared results of direct expanding evaporators with continuous helical and segmental baffles [47]

| Item | LS195Z | LS195Z II |
|---|---|---|
| Compressor type | SRF-3 | |
| Number of condenser tubes | 90 | 90 |
| Total heat transfer area of condenser /$m^2$ | 10.52 | |
| Baffle style | Segmental | Continuous helical |
| Number of evaporator tubes | 196 | 196 |
| Heat transfer area, $m^2$ | 23.99 | 23.91 |
| Refrigeration capacity, kW | 185.8 | 195.0 (+4.9%) |
| Coefficient of performance (COP) | 3.57 | 3.75 (+5.4%) |
| Heat flux on the outer surface, $kWm^{-2}$ | 7.74 | 8.23 |
| Total heat transfer coefficient, W $m^{-2}$ $K^{-1}$ | 1,545 | 1,613 (+4.4%) |

- Continuous helical baffles and combined helical baffles have higher heat transfer coefficients per pressure drop h/Δp than th segmental baffled STHXs. STHX still have higher heat transfer coefficients and much higher pressure drop at the same mass flowrate.
- Continuous helical baffles is superior to discontinuous helica baffle but is more difficult to manufacture (especially when the size is becoming larger).Combined helical baffle is more easier to produce.

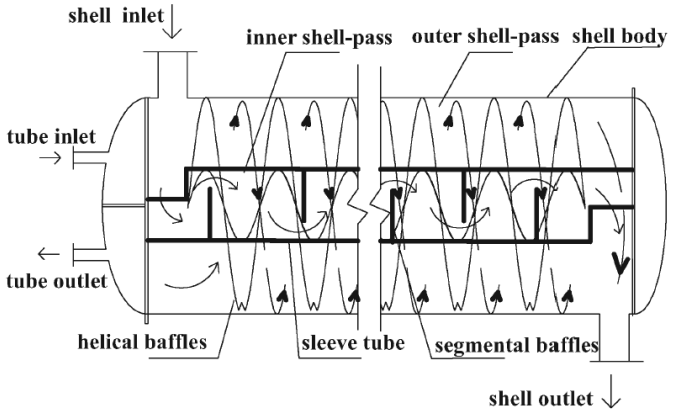


(a) combined parallel multiple shell pass helical baffled STHX [58]

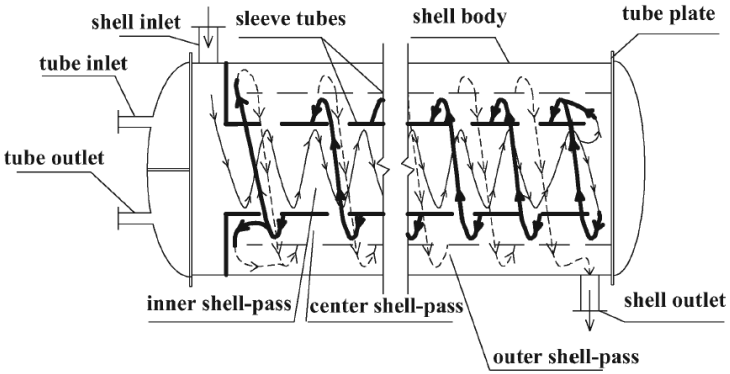


(b) combined serial multiple shell pass STHX with helical baffles [59]

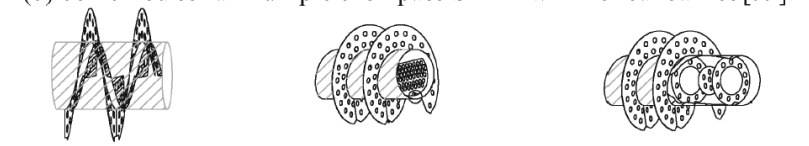


(c) different baffles in inner shell pass [58, 59]

**Figure 18** Schematic of multiple shell pass STHXs with helical baffles.

Surface engineering for phase change heat transfer: A review, *MRS Energy & Sustainability,* pp. 1-40, 2014

- High performance (efficiency) design requires low $\Delta T$

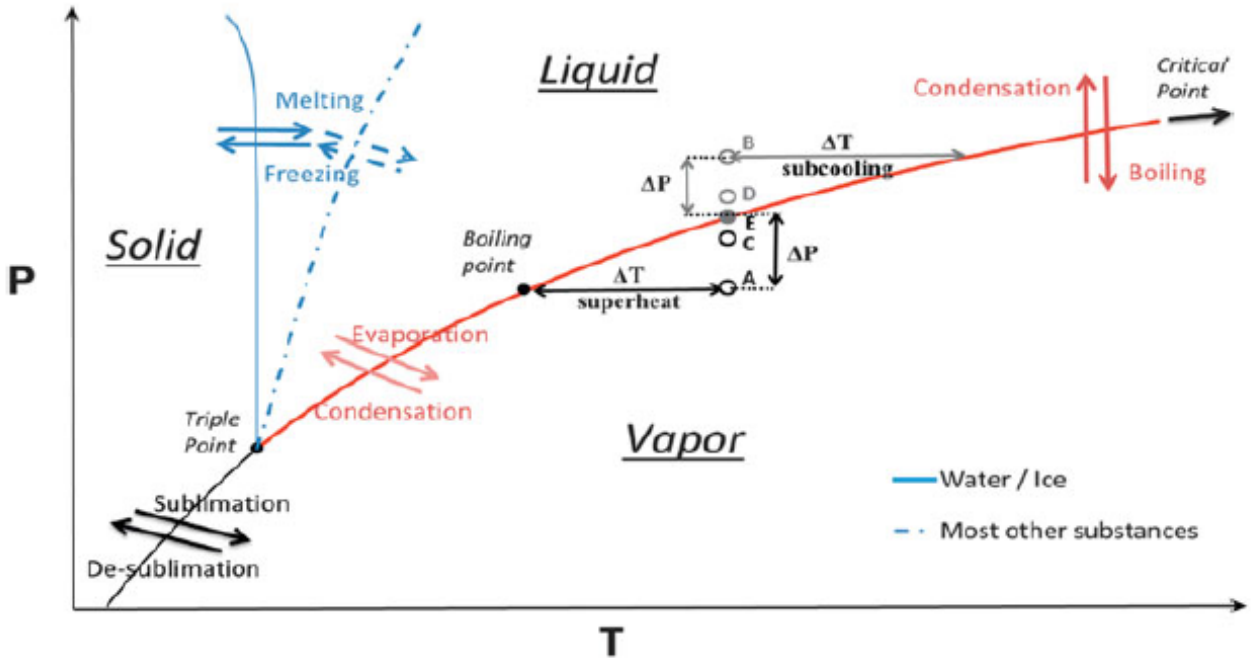


**Figure 3.** The phase change processes considered in this review can all be described in a pressure (log scale) – temperature diagram. The points A, C, and E illustrate the thermodynamic discussion in boiling, section "Characteristics of optimum surfaces for boiling heat transfer", whereas the points B, D, and E are relevant to condensation, section "Characteristics of optimum surfaces for condensation heat transfer."

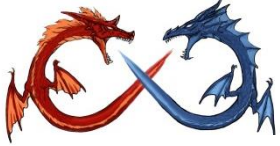

**Table 1.** List of the fluid phases for typical phase change heat transfer processes, with the mechanisms and forces involved.

| | Boiling | Condensation | Desublimation | Freezing |
|---|---|---|---|---|
| Continuous phase | Liquid | Vapor | Vapor | Liquid |
| Discrete phase | Vapor | Liquid | Solid | Solid |
| Wettability that promotes nucleation | Hydrophobic | Hydrophilic | Hydrophilic | Debated |
| Wettability that delays transition from high to low thermodynamic efficiency | Hydrophilic | Hydrophobic | Hydrophobic | Debated |
| Forces that promote discrete phase detachment from substrate | Buoyancy, shear, inertia | Gravity, surface tension, shear | Shear | Inertia, external stress |
| Forces that promote discrete phase attachment to substrate | Surface tension | Surface tension, gravity, inertia | Gravity, surface tension, adhesion | Adhesion |
| Dominant heat transfer mechanism at low $q/\Delta T$ | Single phase convection | Single phase convection | Single phase convection | Single-phase (liquid) convection |
| Dominant heat transfer mechanism at high $q$, below CHF | Multiphase convection | Multiphase convection | Convection (primarily) and conduction | Conduction, convection |
| Dominant mechanism for $q$ above CHF | Radiation | Single phase convection | Conduction | Conduction |

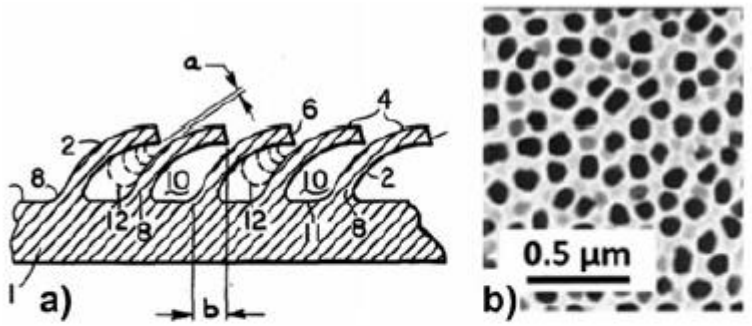


**Figure 8.** Examples of surface machining and roughening: (a) machined surface with bent fins to enhance nucleate boiling, from patent[118]; gap *a* is in the 25–125 μm range; (b) electrochemically processed porous alumina (Anodisc™).

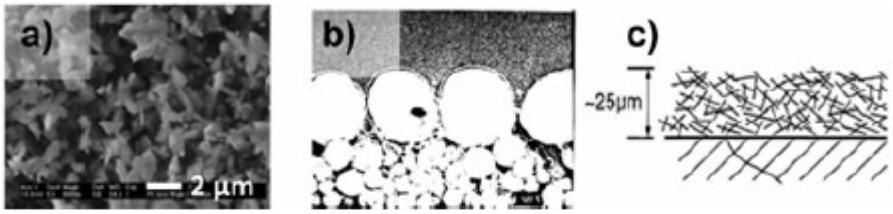


**Figure 9.** Examples of surface coatings: (a) SEM image of an electrospray boron nitride coating, reprinted from Ref. 122, copyright 2011, with permission from Elsevier. (b) Cross-sectional SEM picture of a controlled porous surface fabricated by sintering copper particles of increasing diameters on a copper substrate to study incipient boiling, reprinted from Ref. 123, permission requested from Hemisphere Publishing. The large particles on top are ~250 μm in diameter. (c) Schematic of a porous surface obtained by gluing particles for electronics cooling, from US patent.[124]

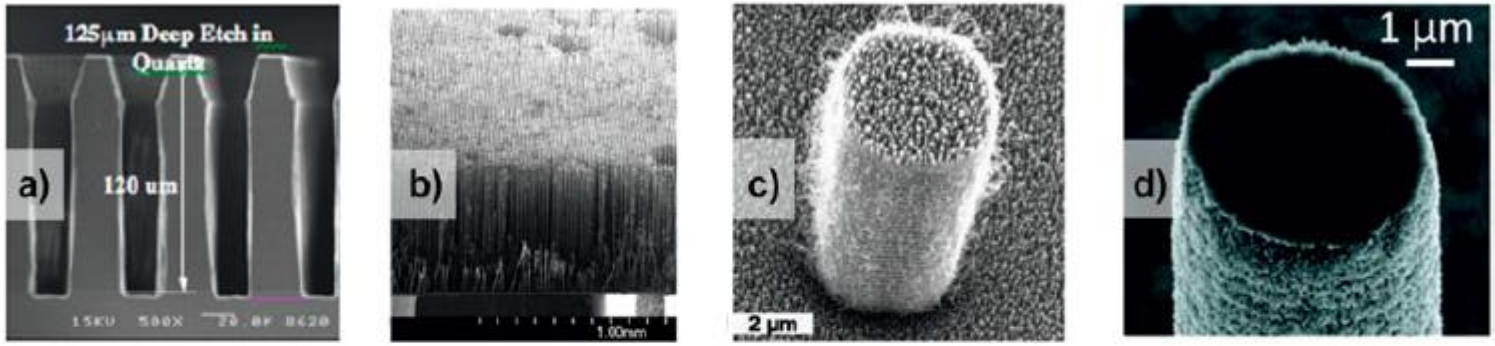


**Figure 10.** Examples of photolithographic processes to create high aspect ratio geometries and multiscale features on solid surfaces. (a) Cross-sectional SEM picture of glass surface textures fabricated by photolithography and deep reactive ion etching on a glass (quartz) substrate. (b) SEM picture of a dense array of 600 μm-tall freestanding Ni posts (diameter = 5 μm; pitch = 14 μm; height-to-diameter aspect ratio = 120) fabricated by electroplating into deep pores formed by photoelectrochemical etching on silicon wafer. Copyright 2011, IEEE. Reprinted with permission from Ref. 128. (c, d) Microscale posts covered with nanoscale features. Figures are reprinted from Refs. 15 and 129 with the permissions of AIP Publishing LLC (Copyright 2007) and the American Chemical Society (copyright 2011), respectively.

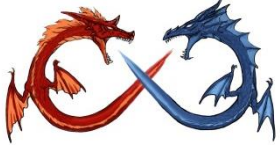

**Table 2.** Microfabrication techniques available for phase change heat transfer applications.

| Category | Processing type | Fabrication method | Distribution of the patterns | Shapes (and size) | Suitable scale of the application | Material |
|---|---|---|---|---|---|---|
| Roughening or machining | Subtractive | Sandpapering, sandblasting | Random | Random (μm) | Large (mass production) | Copper[117] |
| | | Machining | Regular | Controlled (μm to mm) | Medium | Metal[118] |
| | | Chemical, electrochemical | Random | Controlled (10–200 nm) | Medium | Alumina (Anodisc™) |
| Coating | Additive | Sintering | Random | Complex (μm to mm) | Large | Oxide particles[121]; Copper particles on copper[123] |
| | | Electrospraying | Random | Random and complex | Medium | cBN particles on XC–Co[122] |
| | | Gluing | Random | Controlled (1 μm to ~100 μm) | Large | Metal or ceramic particles[124] |
| Lithographic fabrication | Additive or subtractive | Photolithography, e-beam lithography | Regular | Controlled (nm to ~100 μm) | Small | Si pillars on Si[133]; metal pillars on Si[128] |
| | | Interference lithography | Regular | Controlled (100 nm to ~1 μm) | Medium | Si pillars on Si[134]; Ti, Al and Au pillars on glass[135] |


**Figure 12.** The Namib desert beetle features a network of hydrophobic and hydrophilic areas on its back, which have been hypothesized to facilitate collection and transport of water in scarce humidity conditions. Reproduced by permission from Macmillan Publishers Ltd,[188] copyright 2001.

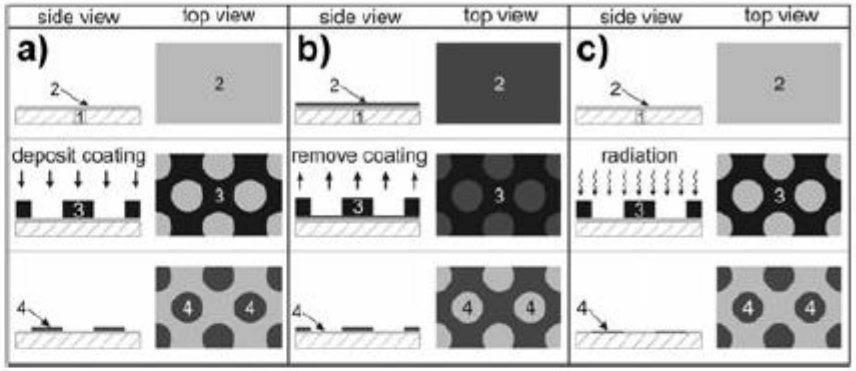


**Figure 14.** Schematics demonstrating three techniques for achieving biphilic surfaces. List of identification numbers: (1) substrate; (2) coating with homogeneous chemistry; (3) mask (e.g., lithography); (4) coating region with differential chemistry as compared with coating (2). In (a), biphilic surfaces are achieved by depositing (4) onto (2); *additive*. In (b), biphilic surfaces are achieved by removing (2) to reveal (4); *subtractive*. In (c), radiation or other reactive mechanisms are utilized to transform the surface chemistry of (2) into (4); *reactive*.

# Fluid Flow and Heat Transfer at Micro- and Meso-Scales With Application to Heat Exchanger Design, Appl. Mech. Rev., **53**, pp. 175–193

Various small and mini heat exchangers in terms of hydraulic diameter $D_h$:

- micro heat exchanger: $D_h$ = 1–100 μm
- meso heat exchanger: $D_h$ = 100 μm–1 mm
- compact heat exchanger: $D_h$ = 1–6 mm
- conventional heat exchanger: $D_h$ > 6 mm

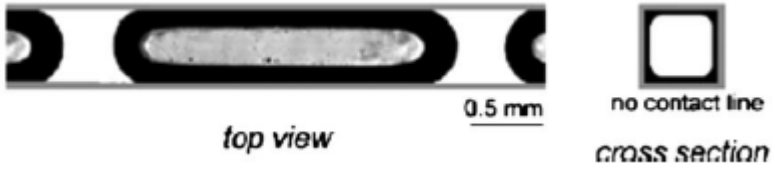


There are several important dimensionless numbers, which are used to represent the feature of fluid flow in microscale channels. According to these dimensionless numbers, the distinction between macro- and microscale channels may be classified as well. Triplett et al. [47] defined flow channels with hydraulic diameters $D_h$ of the order of, or smaller than, the Laplace constant $L$,

$$L = \sqrt{\frac{\sigma}{g(\rho_L - \rho_G)}} \tag{1}$$

as microscale channels, where $\sigma$ is the surface tension, $g$ is the gravitational acceleration, and $\rho_L$ and $\rho_G$ are, respectively, liquid and gas/vapor densities.

Kew and Cornwell [43] earlier proposed the confinement number Co for the distinction of macro- and microscale channels,

$$\mathrm{Co} = \frac{1}{D_h}\sqrt{\frac{4\sigma}{g(\rho_L - \rho_G)}} \tag{2}$$

which is actually based on the definition of the Laplace constant.

Based on a linear stability analysis of stratified flow and the argument that neutral stability should consider a disturbance wavelength of the order of channel diameter, Brauner and Moalem-Maron [48] derived the Eotvös number Eö criterion for the dominance of surface tension for microscale channels,

$$\mathrm{Eö} = \frac{(2\pi)^2\sigma}{(\rho_L - \rho_G)D_h^{\,2}g} > 1 \tag{3}$$

# Two-Phase Flow Patterns and Flow-Pattern Maps: Fundamentals and Applications, Applied Mechanics Reviews 2008, Vol. 61 / 050802-1

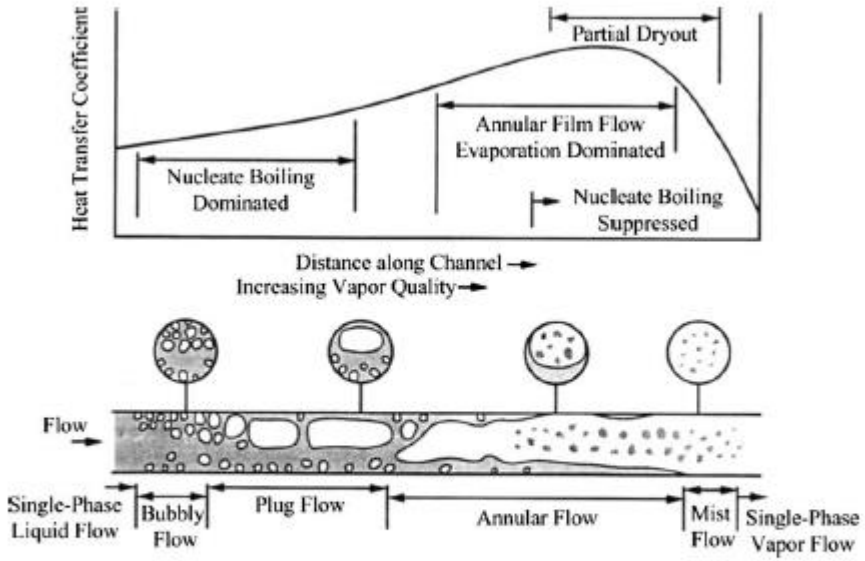


Fig. 4 Schematic of flow patterns and the corresponding heat transfer mechanisms and qualitative variation of the heat transfer coefficients for flow boiling in a horizontal tube [1,2]

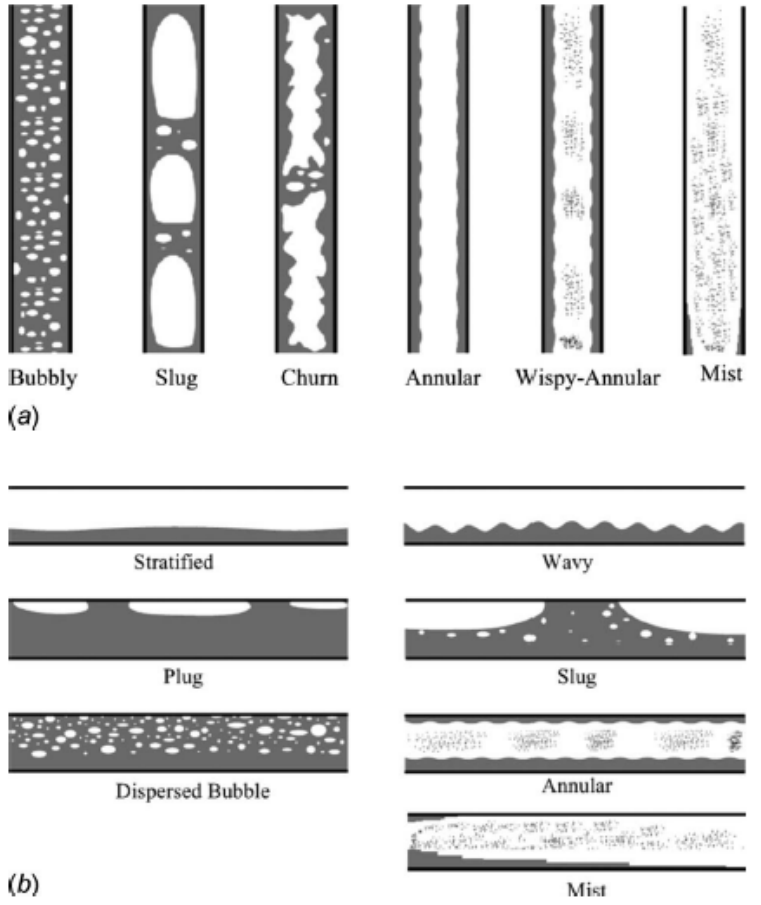


Fig. 2 (*a*) Schematic of flow patterns in vertical upward gas-liquid cocurrent flow; (*b*) schematic of flow patterns in horizontal gas-liquid cocurrent flow [1]

# 微鰭管 Microfin tube

Benefits: increase 100% more heat transfer coefficients with only 10~50% increase of pressure drops

# 熱傳管幾何尺寸

**空調機用熱傳管演進圖**

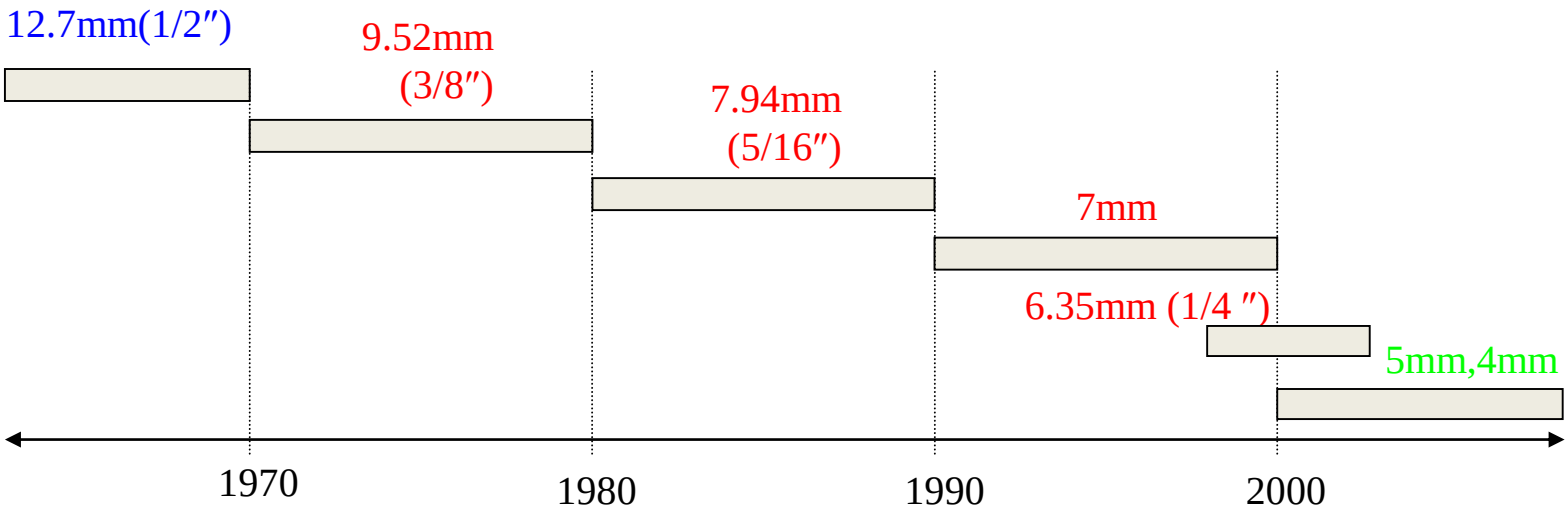


Fig.各種型式的熱傳增強管

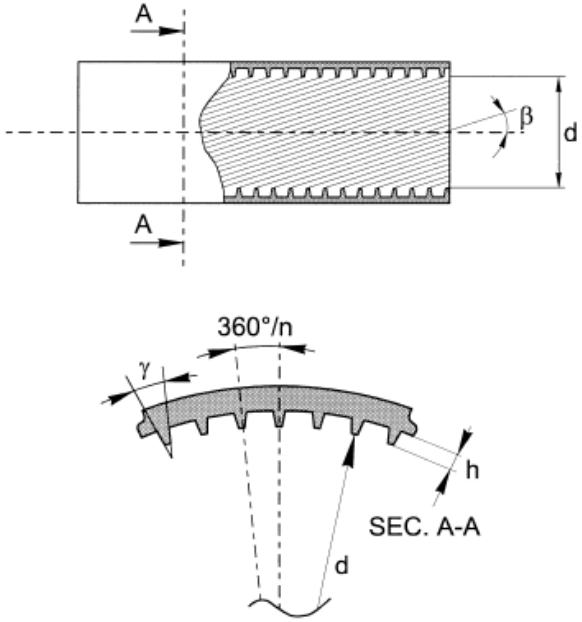


Fig. 1. Characteristic geometrical parameters of inside enhanced tubes.

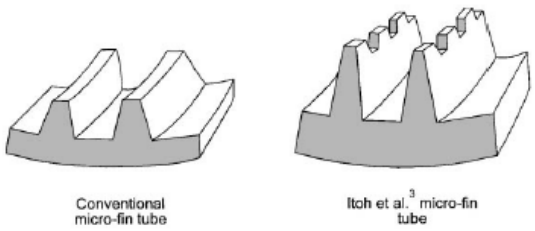


Fig. 3. Comparison between traditional and Itoh et al. [3] micro-fin tube.

*Fig. 3. Comparaison entre les tubes à microailettes classiques et d'Itoh et al. [3].*

Fig. 4. Shape of Muzzio et al. [4] micro-fin tube.

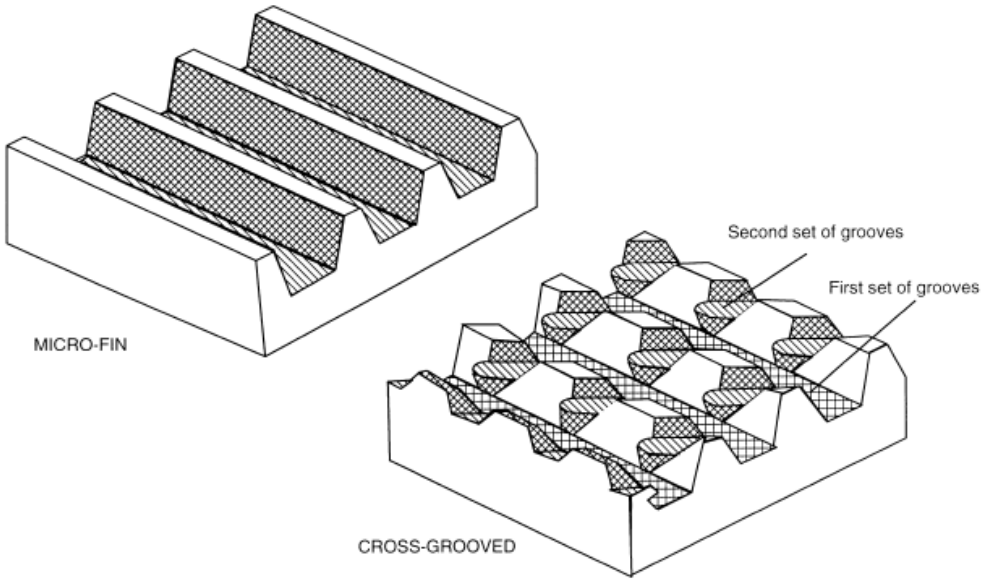


Fig. 2. Typical configuration of micro-fin and cross-grooved surfaces.

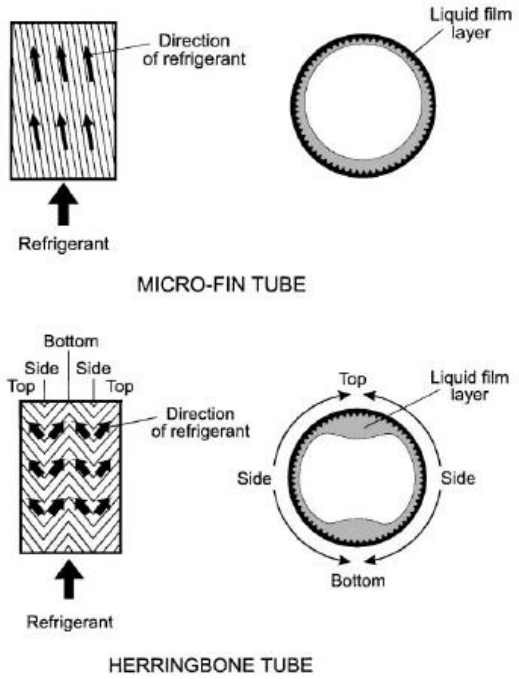


Fig. 5. Comparison between micro-fin and herringbone tubes in annular-type flow pattern.

Heat transfer and pressure drop during condensation of refrigerants inside horizontal enhanced tubes, Int. J. Refrig., 23 (2000) 4-25

# Recent trend in studies for Microfin tube..

- Smaller..
- Low GWP refrigerant
- Refrigerant Mixtures

INTERNATIONAL JOURNAL OF REFRIGERATION 75 (2017) 178–189


## R1234yf condensation inside a 3.4 mm ID horizontal microfin tube

*Andrea Diani, Alberto Cavallini, Luisa Rossetto* *

INTERNATIONAL JOURNAL OF REFRIGERATION 47 (2014) 105–119


## R1234ze(E) flow boiling inside a 3.4 mm ID microfin tube

*Andrea Diani, Simone Mancin*, Luisa Rossetto*

INTERNATIONAL JOURNAL OF REFRIGERATION 69 (2016) 272–284

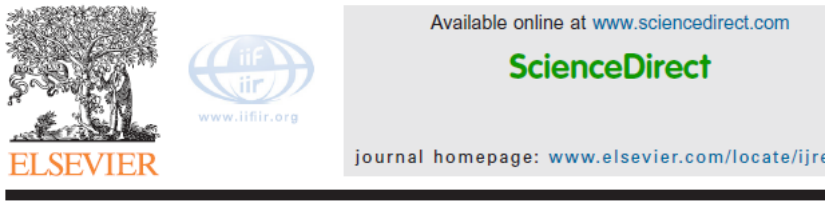


## Experimental investigation of R1234ze(E) flow boiling inside a 2.4 mm ID horizontal microfin tube

*Andrea Diani* [a], *Simone Mancin* [b], *Alberto Cavallini* [a], *Luisa Rossetto* [a,*]

Experimental Thermal and Fluid Science 66 (2015) 127–136

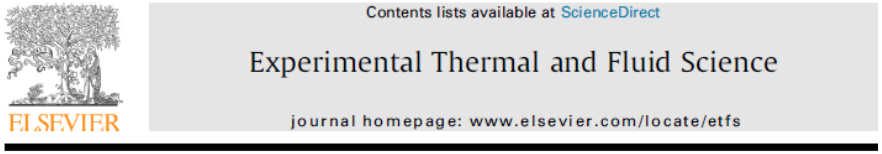


## Flow boiling heat transfer of R1234yf inside a 3.4 mm ID microfin tube

A. Diani [a], S. Mancin [b], L. Rossetto [a,*]

INTERNATIONAL JOURNAL OF REFRIGERATION 33 (2010) 655–663


## Flow boiling heat transfer of carbon dioxide inside a small-sized microfin tube

*Chaobin Dang*, Nobori Haraguchi, Eiji Hihara*

- Recommended correlations applicable for microfin tubes in single phase, condensation, and convective boiling is shown in the review article.

*Heat Transfer Engineering*, 36:582–595, 2015

ISSN: 0145-7632 print / 1521-0537 online
DOI: 10.1080/01457632.2014.939531

Taylor & Francis
Taylor & Francis Group

# Heat Transfer Correlations for Single-Phase Flow, Condensation, and Boiling in Microfin Tubes

*Science and Technology for the Built Environment* (2016) **22**, 1090–1103
ISSN: 2374-4731 print / 2374-474X online
DOI: 10.1080/23744731.2016.1186460

Taylor & Francis
Taylor & Francis Group

# Horizontal convective boiling of R448A, R449A, and R452B within a micro-fin tube

- R410A (GWP=1725) and R404A (GWP=3300)
- Three new refrigerants, R448A (GWP=1274), R449A (GWP=1283), and R452B (GWP=676) , are potential low GWP replacements for R404A (R125/143a/134a [44/52/4]).
- R452B is also a proposed replacement for R410A (R32/125 [50/50])
- R452B (R32/125/1234yf [67/7/26]) are essential for the evaluation of their use for unitary application.

**Table 2**
Characteristics of refrigerants selected [20].

| | R404A | R448A | Rel. dev. |
|---|---|---|---|
| ODP/$GWP_{100\text{-}yr}$ | 0/3943 | 0/1390 | |
| ASHRAE Safety Class | A1 | A1 | |
| Glide[a] (K) | 0.75 | 6.27 | |
| Critical Pressure (kPa) | 345.20 | 356.81 | 3% |
| Critical Temperature (K) | 3728.85 | 4674.93 | 25% |
| NBP (K) | 227.41 | 233.05 | 2% |
| Liquid density[a] (kg $m^{-3}$) | 1150.59 | 1192.39 | 4% |
| Vapour density[a] (kg $m^{-3}$) | 30.32 | 22.09 | −27% |
| Liquid $c_p$[a] (kJ $kg^{-1}$ $K^{-1}$) | 1.39 | 1.42 | 2% |
| Vapour $c_p$[a] (kJ $kg^{-1}$ $K^{-1}$) | 1.00 | 0.98 | −2% |
| Liquid therm. cond.[a] (W $m^{-1}$ K) | $73.15 \cdot 10^{-3}$ | $92.41 \cdot 10^{-3}$ | 26% |
| Vapour therm. cond.[a] (W $m^{-1}$ K) | $12.82 \cdot 10^{-3}$ | $12.01 \cdot 10^{-3}$ | −6% |
| Liquid viscosity[a] (Pa $s^{-1}$) | $179.70 \cdot 10^{-6}$ | $188.35 \cdot 10^{-6}$ | 5% |
| Vapour viscosity[a] (Pa $s^{-1}$) | $11.00 \cdot 10^{-6}$ | $11.42 \cdot 10^{-6}$ | 4% |

[a] Temperature = 273 K.

| | |
|---|---|
| **ASHRAE Number** | **R-452B** |
| **Composition** | **HFO/HFC blend** |
| **Boiling Point** | **-60°F (-51°C)** |
| **Critical Temperature** | **169°F (76°C)** |
| **Ozone Depletion Potential** | **0** |
| **AR5 Global Warming Potential** | **676** |
| **ASHRAE Safety Classification** | **A2L** |
| **Temperature Glide** | **~1K** |

**Table 3.** Representative properties from REFPROP (Lemmon et al. 2013).

| | Evaluated at average test conditions for each fluid | | | Evaluated at $T_s = 277.6$ K | | | |
|---|---|---|---|---|---|---|---|
| Refrigerant | $T_d - T_b$ (K) | $k_l$ (W $m^{-1}$ $K^{-1}$) | Pr | $\sigma$ (mN $m^{-1}$) | $\rho_l$ (kg $m^{-3}$) | $\rho_v$ (kg $m^{-3}$) | $[P_s]_{xq=0}$ (kPa) |
| R404A | 0.50 | 0.074 | 3.5 | 7.05 | 1132.8 | 35.8 | 700.6 |
| R410A | 0.11 | 0.100 | 2.3 | 8.38 | 1151.9 | 34.6 | 920.5 |
| R448A | 5.74 | 0.088 | 2.9 | 9.73 | 1180.7 | 28.8 | 717.1 |
| R449A | 5.39 | 0.090 | 2.9 | 9.53 | 1180.2 | 26.0 | 708.2 |
| R452B | 1.24 | 0.110 | 2.1 | 10.1 | 1072.5 | 28.1 | 889.7 |

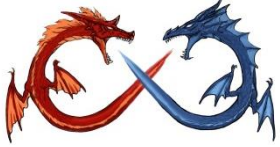

- The heat transfer coefficient for R449A was approximately 8% larger than that for R448A, while the heat transfer coefficient for R452B was more than 59% larger than either R448A or R449A.
- The heat transfer coefficients for R448A and R449A were roughly between 26 and 48% less than that of R404A for the example case.
- In contrast, the model predicts that the R452B heat transfer coefficient was approximately 13% larger than that of R404A for the same conditions.

# 潤滑油的影響

- 在冷凍或熱泵系統的蒸氣壓縮過程中，潤滑是非常必要的。
  - 滑動部位密封和氣瓶閥門減震
- 在空調或冷凍系統中
  - 少量的潤滑油可能會從壓縮機遷移至另一個系統的一部份，改變冷媒的熱傳和摩擦特性
- 作為壓縮機的冷卻液
  - 從軸承和機械元件傳熱到曲軸箱，並且減輕來自運動部件的噪音
- 影響冷媒的熱力及流動性質，尤其是冷媒會顯著改變以下性質
  - 黏滯力
    - 高於冷媒約二到三個冪次
  - 表面張力
    - 高於冷媒約一個冪次
- 在熱傳的特性造成一個顯著的影響

Models of thermodynamic and transport properties of POE VG68 and R410A/POE VG68 mixture. Frontiers of Energy, and Power Engineering in China 2008;2(2):227–34.

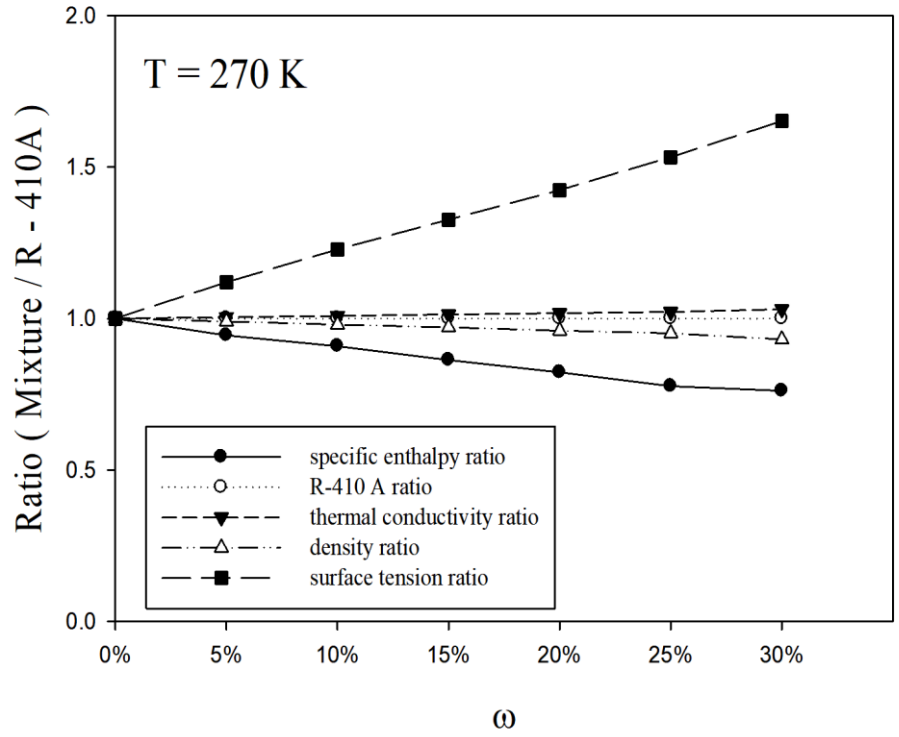


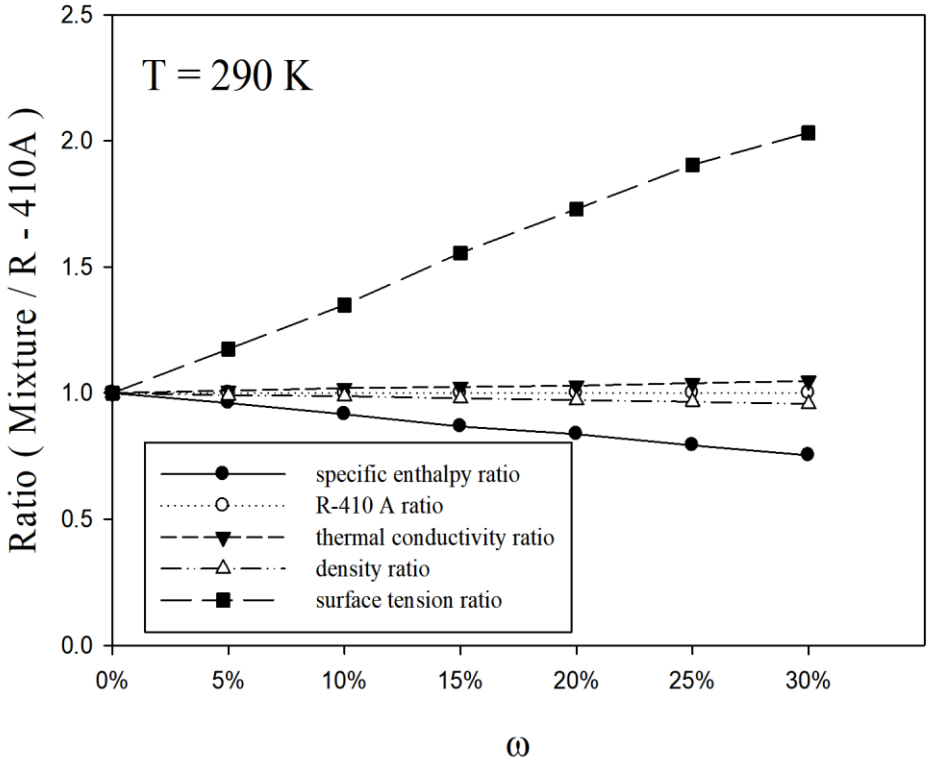


Schematic of the associated properties of R-410A/POE VG68 mixture based on the calculated results.

# Test results for Ji et al.

Nucleate pool boiling heat transfer of R134a and R134a-PVE lubricant mixtures on smooth and five enhanced tubes. Journal of Heat Transfer 2010;132 111502-1-8.

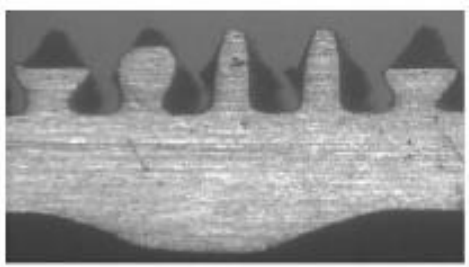
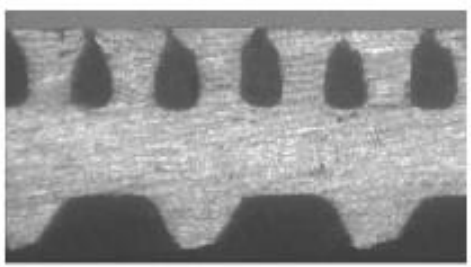
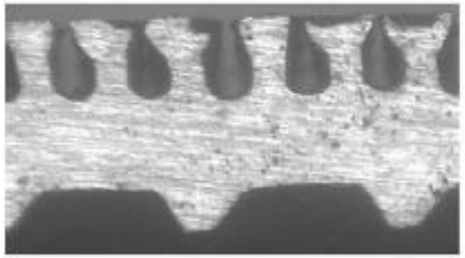
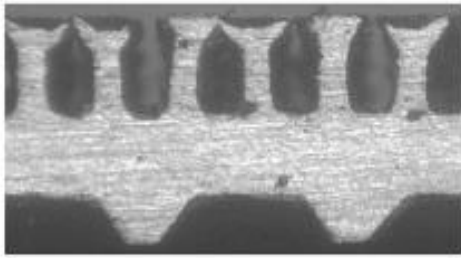

#1, 1435 fins/m #2, 1561 fins/m #3, 1696 fins/m #4, 1761 fins/m

Schematic of the enhanced tube structure by Ji et al.

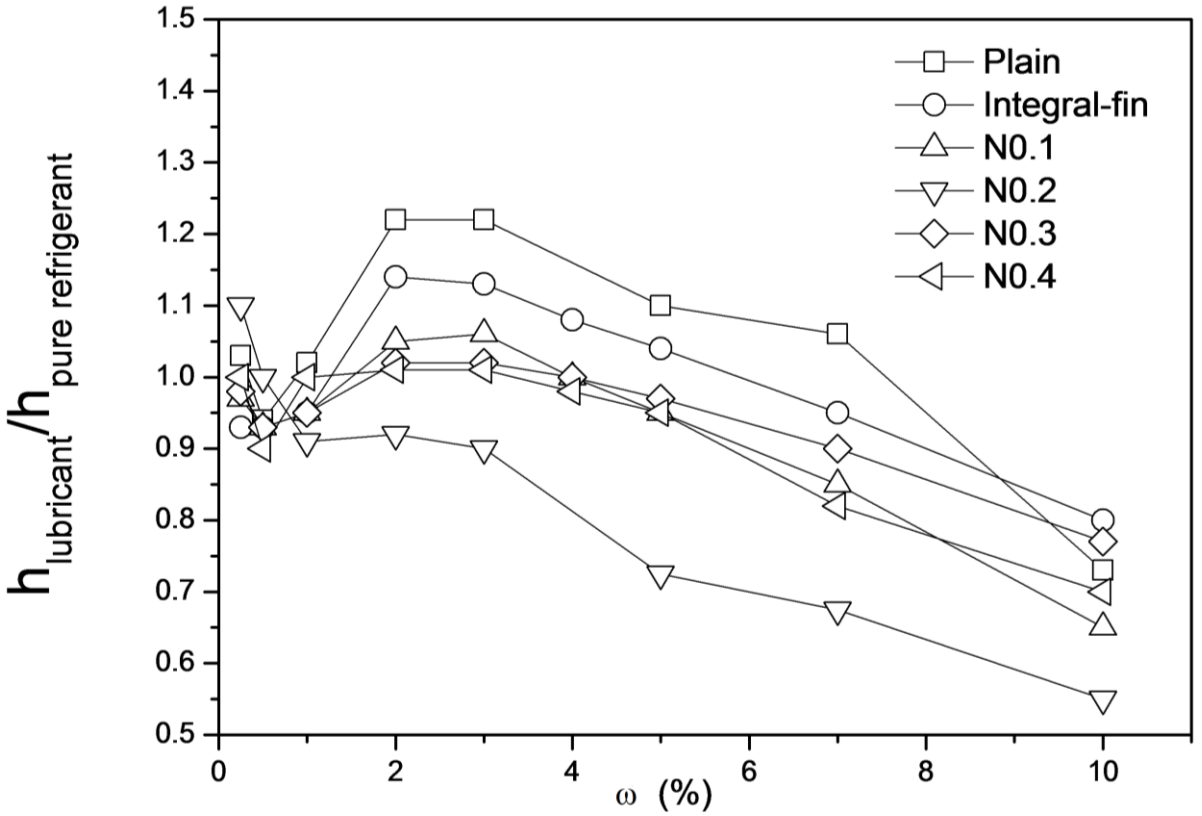

Memory S, Sugiyama DC, Marto PJ. Nucleate pool boiling of R-114 and R-114-oil mixtures from smooth and enhanced surfaces-I. Single tubes. International Journal of Heat and Mass Transfer 1995;38(8):1347–61.
Memory S, Sugiyama DC, Marto PJ. Nucleate pool boiling of R-114 and R-114-oil mixtures from smooth and enhanced surfaces-II. Tube bundles. International Journal of Heat and Mass Transfer 1995;38(8):1363–76.

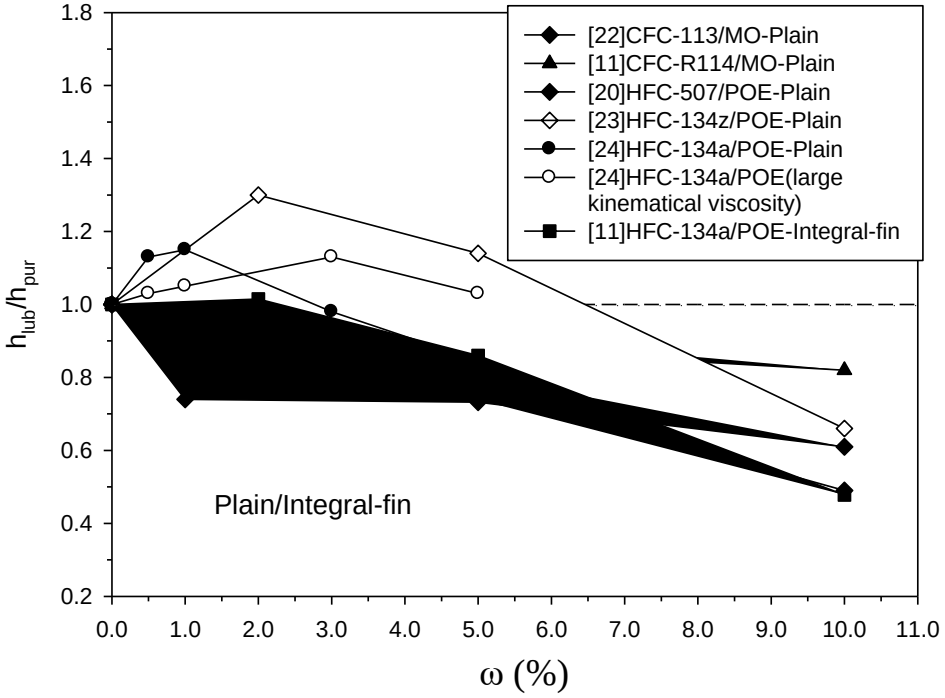


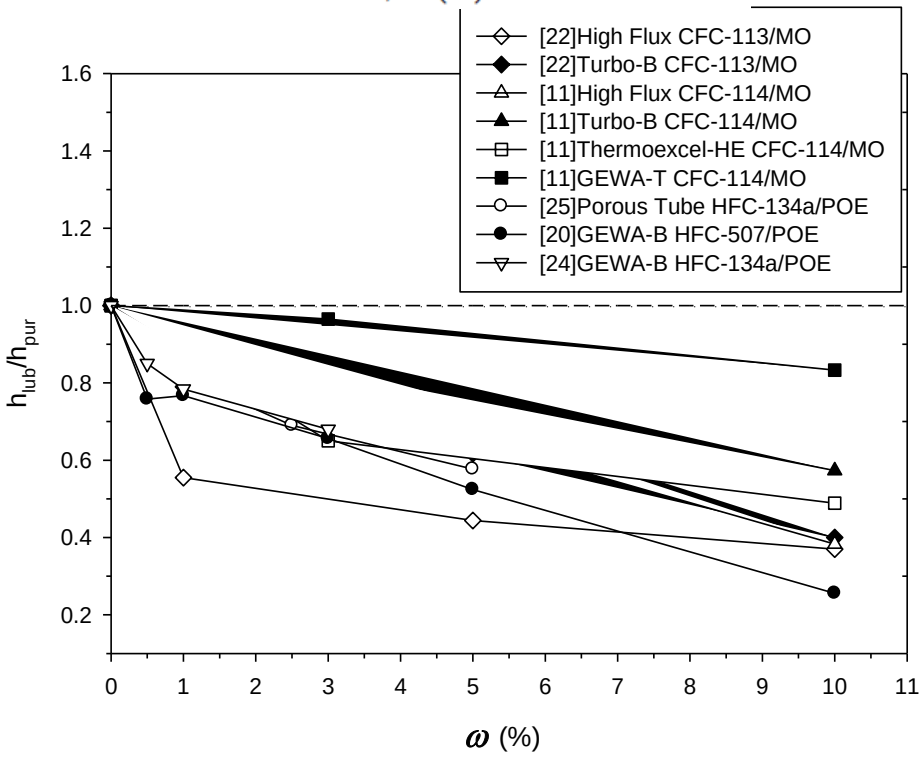


Plain/integral tube

Highly structured tube

**Variation in the relative boiling heat transfer coefficient of lubricant-mixed refrigerant reported in literatures**

Zhu Y, Hu H, Ding G, Peng H, Huang X, Zhuang D, et al. Influence of oil on nucleate pool boiling heat transfer of refrigerant on metal foam covers. International Journal of Refrigeration 2011;34:509–17.

- 在90%至98%不等的金屬泡沫進行核沸騰與孔隙度試驗，並在R-113/VG68平板顯示了相反的趨勢

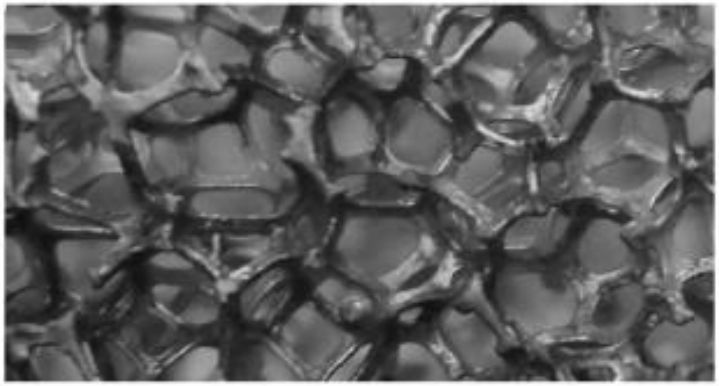

**b** Copper foam #2: ppi=10, Porosity=95%

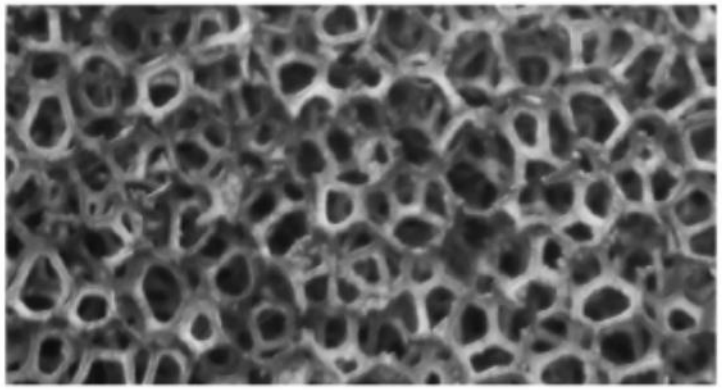

**c** Copper foam #3: ppi=20, Porosity=98%

# 黏度的影響

Worsoe-Schmidt P. Some characteristics of flow pattern and heat transfer of Freon-12 evaporating in horizontal tubes. International Journal of Refrigeration 1960;3(2):40–4.

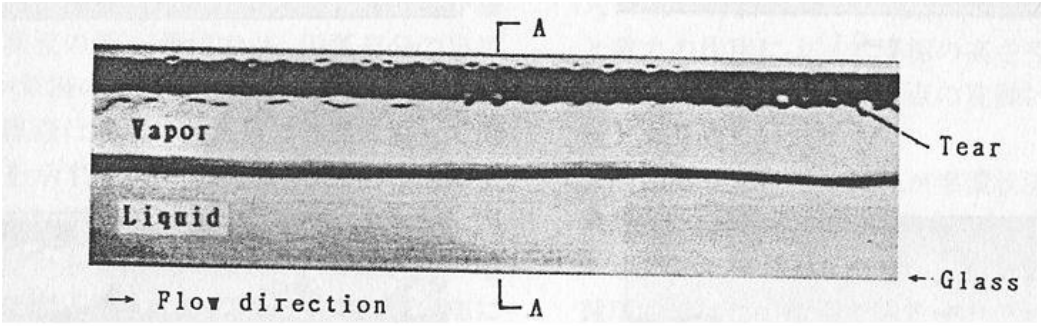


CFC12-oil mixture
G = 110 kg / ($m^2$ • s)
ω = 7 %, x = 0.05

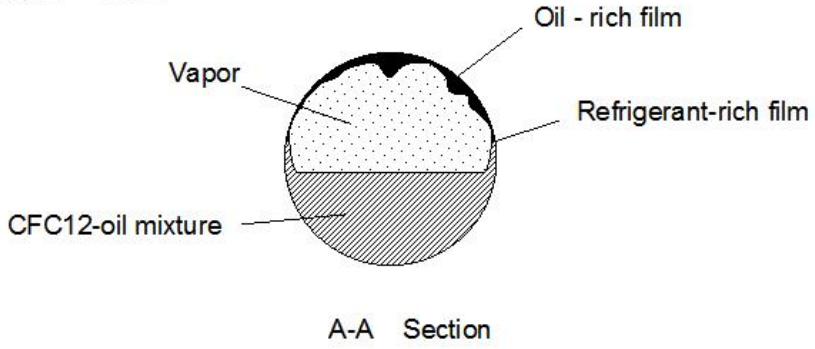


A-A Section

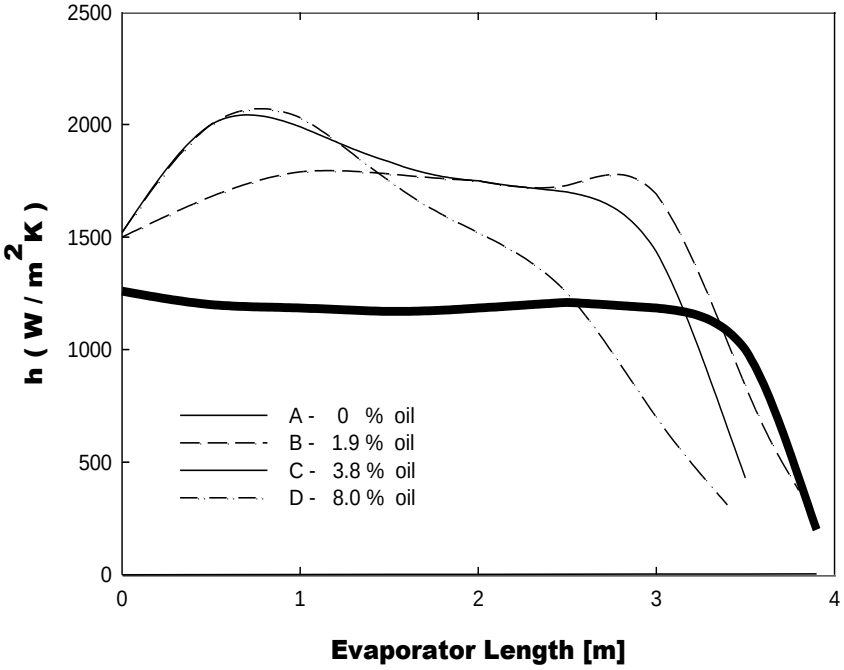


**Schematic of the two-phase annular flow pattern of R-12/oil mixtures with oil-rich tear flow pattern at the upper part of the tube**

# 管的幾何形狀的影響

- 即使在低質量流速，微鰭管也會促進環狀流
- 相對平滑管中冷媒的潤滑油可能會失去促成環狀流的效益
- 在較小的傳熱管中，即使是平滑管，也較容易形成環狀流，因此油存在的可能增益也隨之減小

International Journal of Heat and Mass Transfer 52 (2009) 870–879

# 潤滑油對$CO_2$熱傳特性之影響

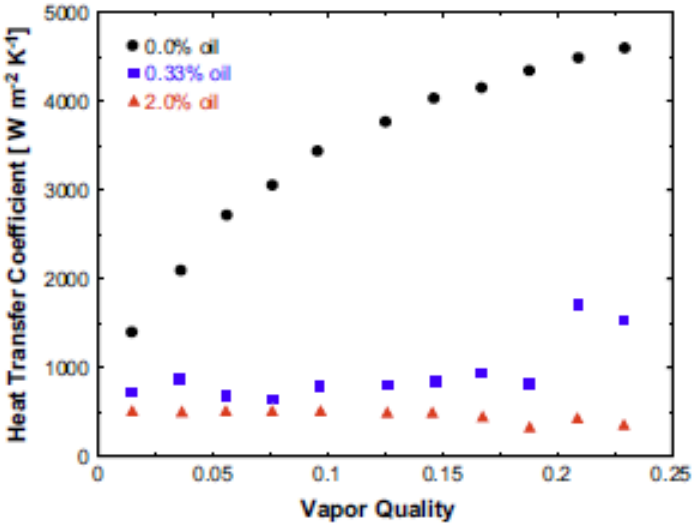


Fig. 5 – The lubricant oil effect on heat transfer coefficient in flow boiling, according to the data of Chaddock and Buzzard (1986) for the test conditions: $G = 65\ kg\,s^{-1}\,m^{-2}$, $q = 6.3\ kW\,m^{-2}$ and $T_{sat} = 9.5\ °C$ at several oil

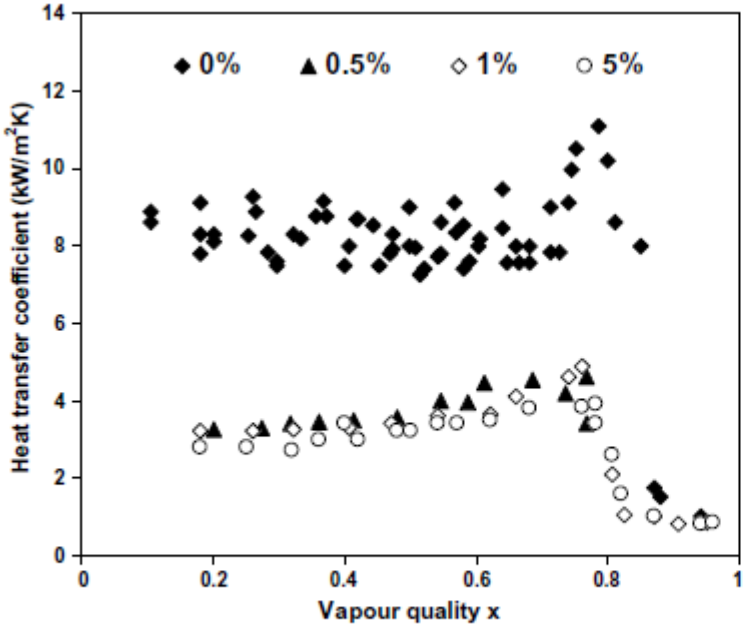


Fig. 1. Effect of oil concentration on $h_{tp}$ of $CO_2$–PAG mixture (Dang et al. [32]) at $G = 360\ kg/m^2\,s$, $T_{sat} = 10\ °C$ and $q = 9\ kW/m^2$.

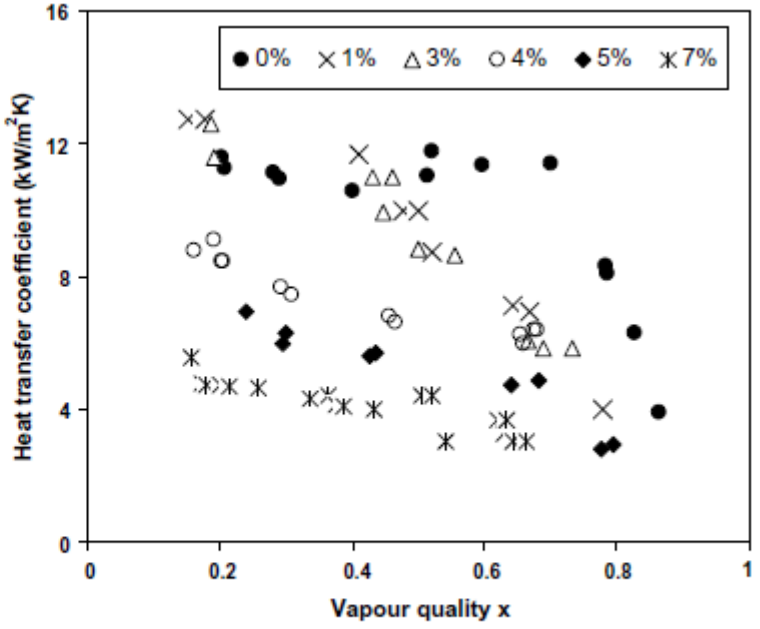


Fig. 3. Effect of oil concentration on $h_{tp}$ (Zhao et al. [38]) at $G = 300\ kg/m^2\,s$, $T_{sat} = 10\ °C$ and $q = 11\ kW/m^2$.

# 潤滑油對$CO_2$熱傳特性之影響 - 平滑管

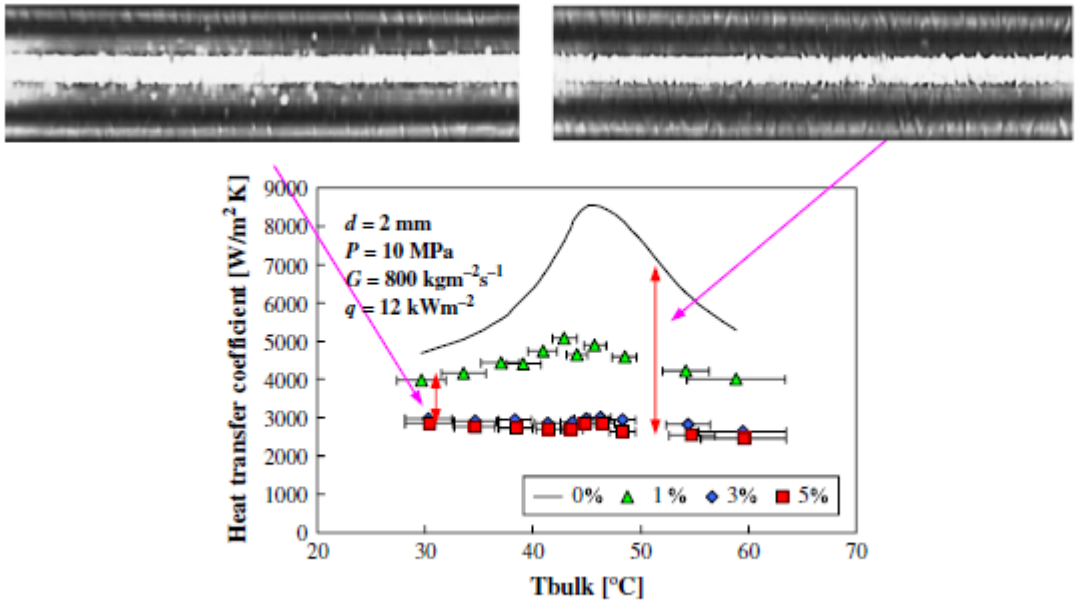


Fig. 9 – Flow pattern of $CO_2$–oil and heat transfer coefficient for 2 mm ID tube.

## PAG type oil

Oil layer effect mainly @ 1~3%

Higher mass flux cause considerably degradation (droplet vs. film)

INTERNATIONAL JOURNAL OF REFRIGERATION 31 (2008) 1265–1272

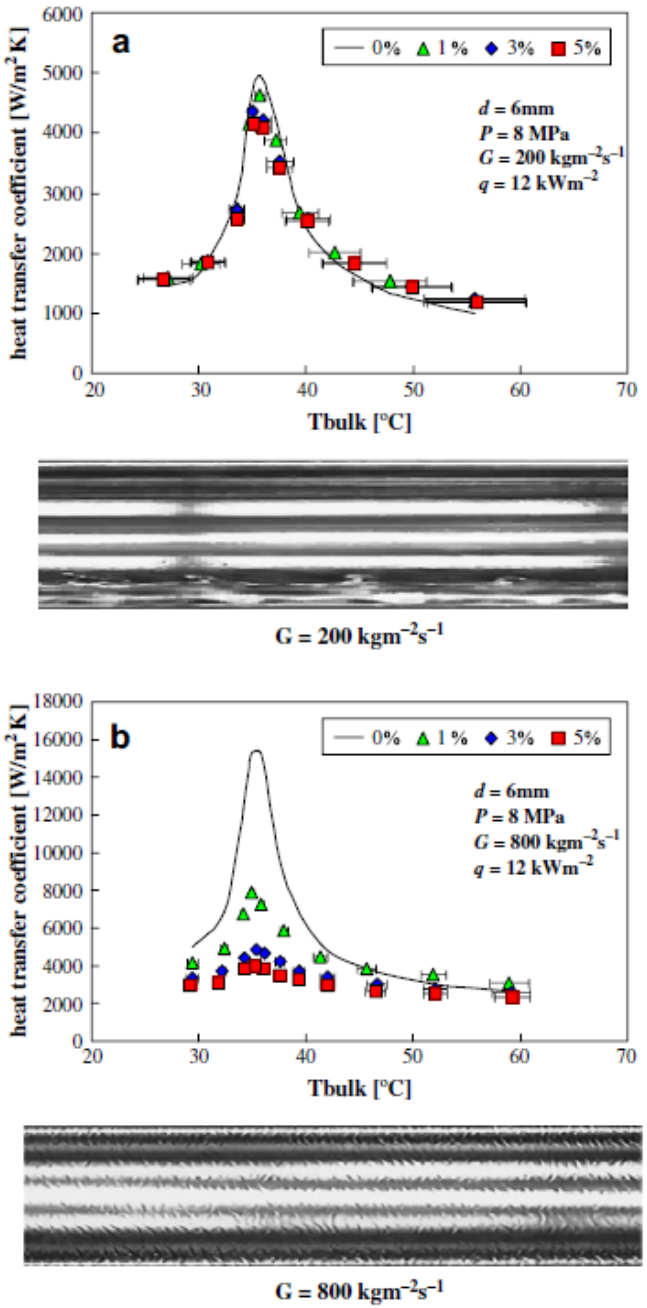


Fig. 10 – Flow pattern of $CO_2$–oil (40 °C) and heat transfer coefficient for 6 mm ID tube.

# 潤滑油對$CO_2$熱傳特性之影響 - 微鰭管

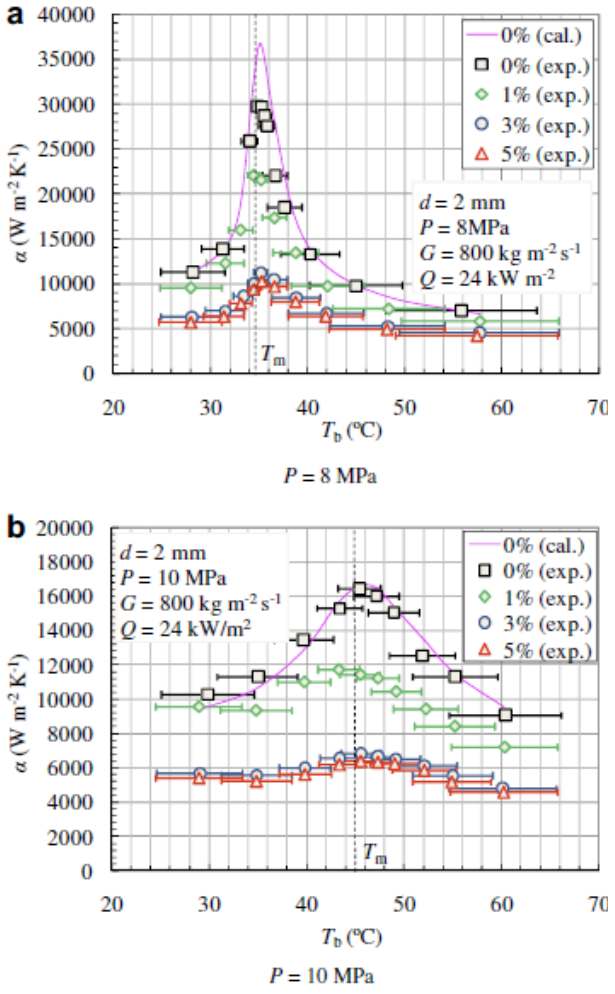


Fig. 7 – Change in $\alpha$ with $T_b$ at different x values.

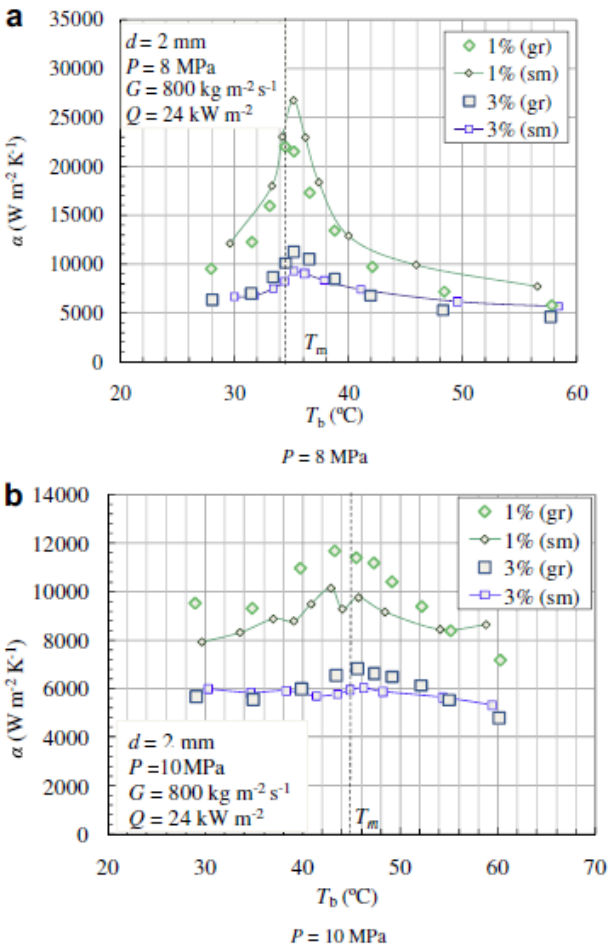


Fig. 8 – Comparison between the $\alpha$ values obtained for the grooved tube and smooth tube at $G = 800\ kg\ m^{-2}\ s^{-1}$.

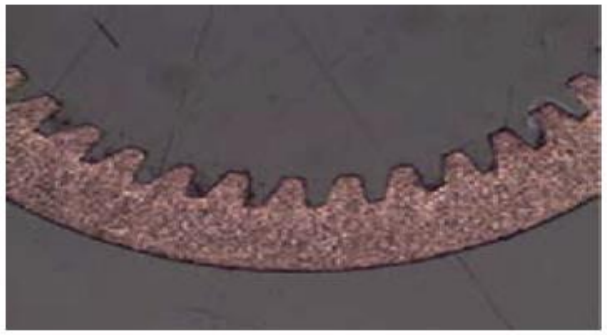

Fig. 2 – Enlarged view of cross-sectional shape of grooved tube.

**Table 1 – Specifications of internally GROOVED tube.**

| | | | |
|---|---|---|---|
| O.D. [mm] | 2.646 | I.D. [mm] | 1.996 |
| Wall thickness [mm] | 0.269 | Fin height [mm] | 0.117 |
| Apex angle [°] | 34.8 | Helix angle [°] | 6.3 |
| Number of fins | 40 | Area enlargement ratio | 2.0 |

Less effect of oil for microfin helps to break up the oil film

# $CO_2$ 流動流譜 (潤滑油)

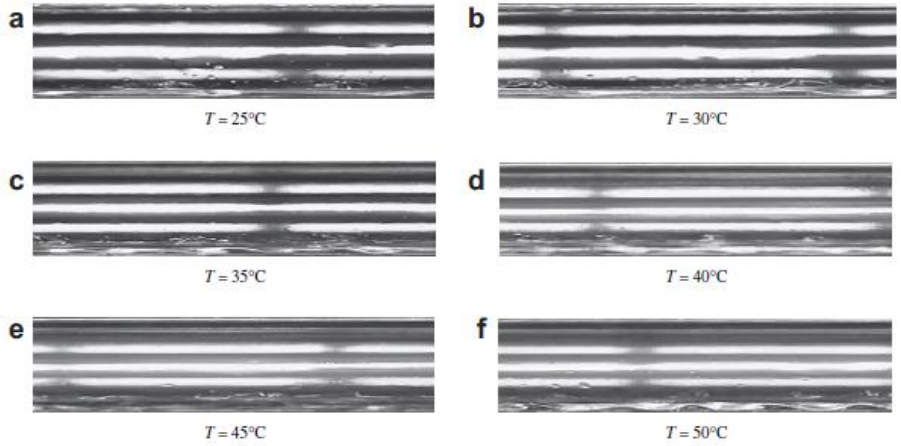


Fig. 6 – Comparison of flow pattern at different temperature for 6 mm ID tube; $d = 6$ mm, $P = 8$ MPa, $G = 200$ kg m$^{-2}$ s$^{-1}$, $x = 1\%$.

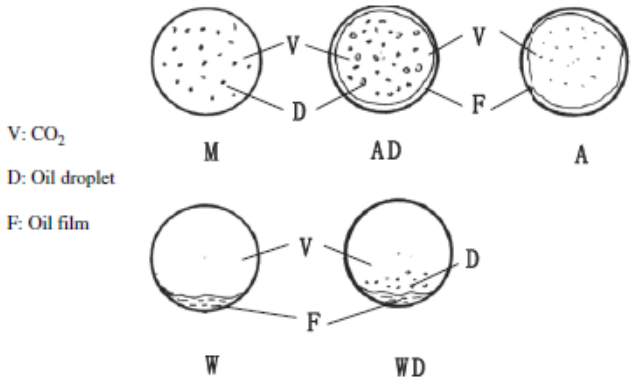


Fig. 4 – Classification of flow pattern. M: mist flow; AD: annular-dispersed flow; A: annular flow; W: wavy flow; WD: wavy-dispersed flow.

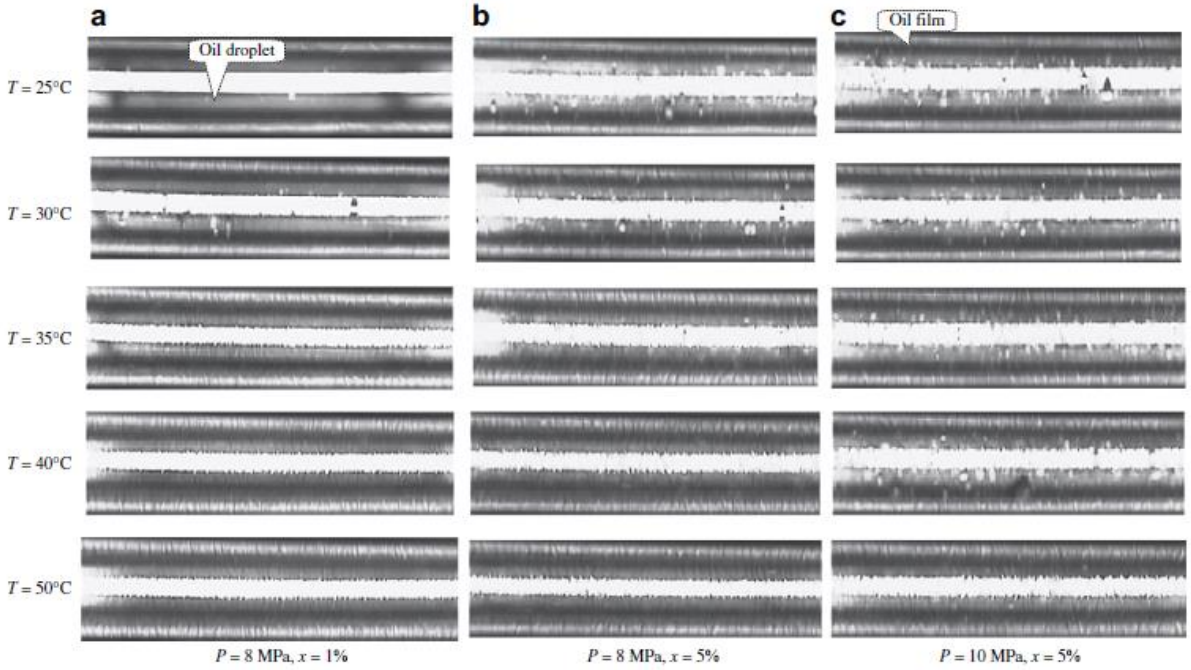


Fig. 5 – Flow visualization of $CO_2$ with entrained PAG oil; $d = 2$ mm, $G = 800$ kg m$^{-2}$ s$^{-1}$.

# Conclusions

- 推薦Webb教授熱交換器性能的評價方法，評估熱傳性能有效改善，必須要有基本熱傳與壓降的數據。
- 熱傳型能的提升
  - $A\uparrow > h\uparrow > \Delta T\uparrow$
  - 增加面積有很多的side effect，與熱交換器型式及流體機械的使用有關聯
- 熱傳增強性能與流動型態有絕對的關係，相變化時差異尤其大，熱傳管的選取與評估應事先根據使用的工作流體、工作條件、流型轉換等因素的影響來考量
- 各式熱傳增強的開發與選擇仍需輔佐精確的實驗驗證
- 細徑化與LGWP冷媒為先今冷凍空調應用之傳熱管發展之重要方向
- 潤滑油對沸騰熱傳有相當的影響，使用上要特瞭解該油品與冷媒混合後的特性

# 感謝聆聽

## 敬請賜教

王啟川
Tel: +886-3-5712121 ext. 55105
E-mail:ccwang@mail.nctu.edu.tw